Am J Physiol Heart Circ Physiol 297: H1504–H1513, 2009.
First published August 14, 2009; doi:10.1152/ajpheart.00194.2009.

Postinfarction gene therapy with adenoviral vector expressing decorin mitigates cardiac remodeling and dysfunction

Longhu Li,[1] Hideshi Okada,[1] Genzou Takemura,[1] Ken-ichiro Kosai,[2] Hiromitsu Kanamori,[1] Masayasu Esaki,[1] Tomoyuki Takahashi,[3] Kazuko Goto,[1] Akiko Tsujimoto,[1] Rumi Maruyama,[1] Itta Kawamura,[1] Tomonori Kawaguchi,[1] Toshiaki Takeyama,[1] Takako Fujiwara,[4] Hisayoshi Fujiwara,[1] and Shinya Minatoguchi[1]

[1]*Division of Cardiology, Gifu University Graduate School of Medicine, Gifu;* [2]*Department of Gene Therapy and Regenerative Medicine, Kagoshima University Graduate School of Medical and Dental Sciences, Kagoshima;* [3]*Division of Gene Therapy and Regenerative Medicine, Cognitive and Molecular Research Institute of Brain Diseases, Kurume University, Kurume; and* [4]*Department of Food Science, Kyoto Women's University, Kyoto, Japan*

Submitted 2 March 2009; accepted in final form 12 August 2009

Li L, Okada H, Takemura G, Kosai K, Kanamori H, Esaki M, Takahashi T, Goto K, Tsujimoto A, Maruyama R, Kawamura I, Kawaguchi T, Takeyama T, Fujiwara T, Fujiwara H, Minatoguchi S. Postinfarction gene therapy with adenoviral vector expressing decorin mitigates cardiac remodeling and dysfunction. *Am J Physiol Heart Circ Physiol* 297: H1504–H1513, 2009. First published August 14, 2009; doi:10.1152/ajpheart.00194.2009.—The small leucine-rich proteoglycan decorin is a natural inhibitor of transforming growth factor-β (TGF-β) and exerts antifibrotic effects in heart and to stimulate skeletal muscle regeneration. We investigated decorin's chronic effects on postinfarction cardiac remodeling and dysfunction. Myocardial infarction (MI) was induced in mice by left coronary artery ligation. An adenoviral vector encoding human decorin (Ad.CAG-decorin) was then injected into the hindlimbs on *day 3* post-MI (control, Ad.CAG-LacZ). Four weeks post-MI, the decorin-treated mice showed significant mitigation of the left ventricular dilatation and dysfunction seen in control mice. Although infarct size did not differ between the two groups, the infarcted wall thickness was greater and the segmental length of the infarct was smaller in decorin-treated mice. In addition, cellular components, including myofibroblasts and blood vessels, were more abundant within the infarcted area in decorin-treated mice, and fibrosis was significantly reduced in both the infarcted and noninfarcted areas of the left ventricular wall. Ten days post-MI, there was greater cell proliferation and less apoptosis among granulation tissue cells in the infarcted areas of decorin-treated mice. The treatment, however, did not affect proliferation and apoptosis of salvaged cardiomyocytes. Although decorin gene therapy did not affect TGF-β1 expression in the infarcted heart, it inhibited Smad2/3 activation (downstream mediators of TGF-β signaling). In summary, postinfarction decorin gene therapy mitigated cardiac remodeling and dysfunction by altering infarct tissue noncardiomyocyte dynamics and preventing cardiac fibrosis, accompanying inhibition of Smad2/3 activation.

heart failure; myocardial infarction; transforming growth factor-β

CHRONIC HEART FAILURE HAS emerged as a leading cause of mortality and morbidity worldwide. At present, patients with chronic heart failure have a poor prognosis (26) and a high likelihood that they will have to be readmitted to hospital, despite treatment (16, 26). The most common cause of heart failure is myocardial infarction (MI)-induced remodeling of the left ventricle (LV), which is characterized by LV dilatation and diminished cardiac performance (3, 13, 14, 39). Therefore, to improve clinical outcomes among patients with MI, it will be essential to develop therapies that effectively inhibit the resultant LV remodeling.

The most critical determinant of subsequent LV remodeling and eventual heart failure is the magnitude of the acute MI, which can be determined within several hours of an attack (41). The process of cardiac remodeling is complicated, however, and many other factors, including late death or hypertrophy of cardiomyocytes, fibrosis, and the expression of various cytokines, are associated with the continued disease progression during the chronic stage (5, 32, 47, 53). Several lines of evidence point to the critical role played by transforming growth factor-β (TGF-β) during the progression of myocardial fibrosis, suggesting that TGF-β plays a critical role during the healing process following MI and thus affects cardiac remodeling and function during the chronic stage (10, 17, 29). Soluble TGF-β type II receptor (sTβRII) inhibits the action of TGF-β, most likely by adsorbing TGF-β or by acting as a dominant-negative receptor (20). Our laboratory previously reported that the postinfarction gene therapy with adenoviral vector encoding sTβRII mitigated cardiac remodeling and dysfunction at the chronic stage of MI by affecting cardiac fibrosis and infarct tissue dynamics (37). It was thus suggested that a therapy aimed at suppressing TGF-β signaling might represent a new approach to the treatment of post-MI heart failure, applicable during the subacute stage.

Decorin is a small chondroitin-dermatan sulfate proteoglycan, consisting of a core protein and a single glycosaminoglycan chain (25, 43). Importantly, decorin negatively regulates TGF-β by binding it and neutralizing its biological activity, i.e., a natural inhibitor of TGF-β (54). Levels of decorin are reportedly increased in myocardial tissue from patients who have undergone implantation of an LV assist device, which induces regression of fibrosis (21). The most recent study suggests that in vivo transfer of decorin gene promotes skeletal muscle regeneration after injury (28). In the present study, therefore, we hypothesized that postinfarction treatment with decorin may mitigate chronic heart failure by affecting the LV remodeling process. Decorin protein, when intravenously administered, rapidly disappears from the circulation, and ~70% of the dose is trapped by the liver within 10 min (31). Thus a continuous protein supply is necessary to maintain the plasma level of decorin sufficient to display the effect on the target organ, and a gene therapy is appropriate for that purpose.

Address for reprint requests and other correspondence: G. Takemura, Division of Cardiology, Gifu Univ. Graduate School of Medicine, 1-1 Yanagido, Gifu 501-1194, Japan (e-mail: gt@gifu-u.ac.jp).

However, a virus-mediated gene delivery directly into the systemic circulation is potentially harmful, occasionally lethal, through viremia or immune reaction (24, 30). Thus a local gene delivery is more preferable; at the site, decorin is continuously produced and released to the systemic circulation, reaching the heart. Direct injection of therapeutic genes into the heart may be more effective, but we selected less invasive and more feasible method (injection into hindlimb muscles) for gene delivery in the present study. Adenoviruses and adeno-associated viruses are currently the most effective vectors for delivering therapeutic genes in the cardiovascular system (42). In the present study, we initiated adenovirus-mediated transduction of the decorin gene into mouse hindlimb muscles on *day 3* of MI, times at which the therapy does not affect acute ischemic death of cardiomyocytes, and examined its effects on post-MI heart failure at the chronic stage.

MATERIALS AND METHODS

Recombinant adenoviral vectors. The adenoviral vector plasmid pAd-decorin, which harbors the cytomegalovirus immediate-early enhancer, a modified chicken β-actin promoter and human decorin cDNA (Ad.CAG-decorin), was constructed using the in vitro ligation method, as previously described (33). Control adenovirus harboring the LacZ gene (Ad.CAG-LacZ) was prepared as previously described (6).

Evaluation of decorin expression in vitro. HeLa cells were transfected with pHM5-CAG-decorin plasmid using Lipofectamine 2000 (Invitrogen) and cultured for 48 h at 37°C. Levels of human decorin in culture supernatants and in cell lysates were evaluated by Western blotting. In addition, levels of decorin in cultured cells were assessed immunohistochemically using anti-human decorin (R&D Systems) as the primary antibody and Alexa Fluor 488 anti-goat IgG (Invitrogen) as the secondary antibody. Nuclei were stained with 4′,6-diamidino-2-phenylindole. The cells were observed under a laser scanning confocal microscope (LSM510, Zeiss).

Animal experimental protocols. This study was approved by our institutional animal research committee and conformed to the Guide for the Care and Use of Laboratory Animals published by the US National Institutes of Health (National Institutes of Health publication no. 85–23, revised 1996). MI was induced in 10-wk-old male C57BL/6J mice (Japan SLC, Shizuoka, Japan) by ligating the left coronary artery, as previously described (36, 38). Ad.CAG-decorin (1×10^{11} particles per mouse) was then injected into the hindlimb muscles of the mice. As a control, Ad.CAG-LacZ was injected in the same manner. In sham-operated mice, the suture was passed but not tied.

MI was induced in 50 mice. Of those, 34 remained alive on *day 3* post-MI and were entered into the study, randomly assigned to the decorin ($n = 16$) or LacZ ($n = 18$) treatment group, and followed up for 4 wk. Sham-operated mice ($n = 8$) were injected with the same volume of saline in a similar manner and examined 4 wk later. In another experiment, 14 mice were divided into decorin and LacZ treatment groups ($n = 7$ each) on *day 3* post-MI, and the survivors ($n = 5$ in the decorin group and $n = 4$ in the LacZ group) were examined on *day 10* post-MI.

Physiological studies. Echocardiography and cardiac catheterization were performed before death, as previously described (36, 38). Animals were anesthetized with halothane (induction, 2%; maintenance, 0.5%) in a mixture of N_2O and O_2 (0.5 l/min each) via a nasal mask. Echocardiograms were recorded 4 wk post-MI using an echocardiographic system (Vevo770, Visualsonics) equipped with a 45-MHz imaging transducer. The right carotid artery was then cannulated with a micromanometer-tipped catheter (SPR 671, Millar Instrument) that was advanced into the LV via the aorta to record pressures and change in pressure over time.

Histological analysis. After the physiological studies were complete, all surviving mice were euthanized, and their hearts removed. The excised hearts were cut into two transverse slices. The basal specimens were fixed in 10% buffered formalin and embedded in paraffin, after which 4-μm-thick sections were stained with hematoxylin-eosin, Masson's trichrome, and Sirius red F3BA (0.1% solution in saturated aqueous picric acid) (Aldrich). Quantitative assessments of cardiomyocyte size (as the transverse diameter), cell population, and fibrotic area were made using a LUZEX F multipurpose color image processor (Nireco) with 20 randomly chosen high-power fields in each section.

Immunohistochemical analysis. Deparaffinized 4-μm-thick sections were incubated with a primary antibody against human decorin (R&D Systems), complement 9 (C9; Novo Castra) at a dilution of 1:100, α-smooth muscle actin (α-SMA; 1A4) at 1:100, von Willebrand factor (vWF) at 1:100, Ki-67 at 1:25 (all from Dako), or CD45 at 1:100 (Pharmingen), after which they were immunostained using an ABC kit (Vector) with the chromogen diaminobenzidine HCl or immunolabeled with Alexa Fluor 488 or 568 at 1:500 (Molecular Probes). Nuclei were stained with hematoxylin or Hoechst 33342.

Apoptosis was evaluated using the terminal deoxynucleotidyl transferase-mediated in situ nick-end labeling (TUNEL) method with

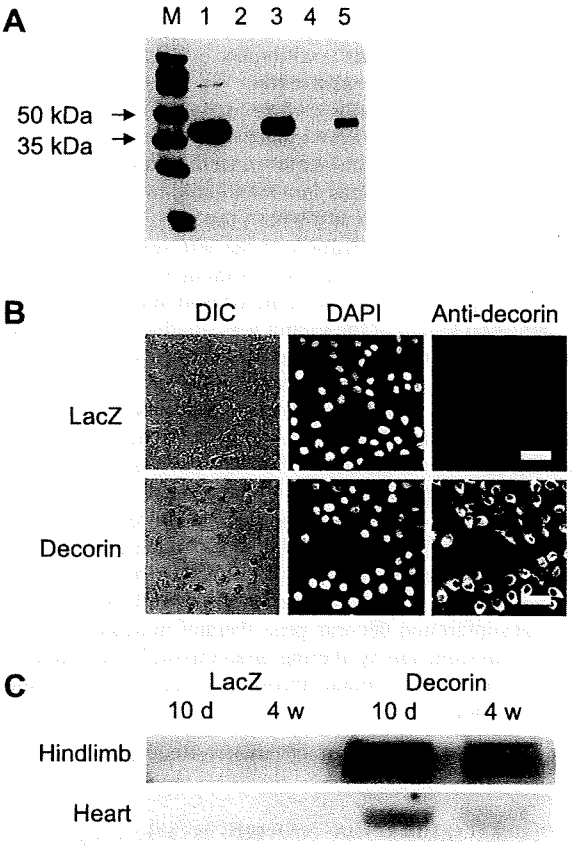

Fig. 1. Expression of decorin in vitro and in vivo through human decorin gene transfer. *A*: Western analysis of human decorin (40 kDa) in Hela cells: M, molecular weight markers; *lane 1*, recombinant decorin (a positive control); *lanes 2* and *3*, total cell lysate from HeLa cells transfected with LacZ (*lane 2*) or decorin (*lane 3*) plasmid; *lanes 4* and *5*, supernatant from Hela cells transfected with LacZ (*lane 4*) or decorin (*lane 5*). *B*: immunohistochemical analysis of human decorin expressed in Hela cells transfected with decorin plasmid. DIC, differential interference contrast image; DAPI, 4′,6-diamidino-2-phenylindole. Scale bars, 20 μm. *C*: Western analysis of human decorin in hindlimb muscle and heart tissue from mice bearing 10-day- or 4-wk-old myocardial infarctions (MIs) following transduction with Ad.CAG-LacZ or Ad.CAG-decorin on *day 3* post-MI.

an ApopTag kit (Chemicon) according to the supplier's instructions. Mouse mammary tissue served as a positive control. For double immunofluorescent labeling, tissue sections were first stained with Fluorescein-FragEL (Oncogene) and then labeled with anti-α-SMA or anti-vWF, followed by Alexa Fluor 568. In addition, to evaluate cell proliferative activity and apoptosis of the salvaged cardiomyocytes, we performed double immunofluorescence for myoglobin (1:1,000), combined with Ki-67 (1:25) or TUNEL. Tissue sections were first stained with anti-Ki-67 followed by Alexa 488 or Fluorescein-FragEL and then labeled with anti-myoglobin antibody (DAKO) followed by Alexa 568. Nuclei were stained with Hoechst 33342. Immunofluorescence preparations were observed under a confocal microscope (LSM510, Zeiss).

Western blotting. Proteins extracted from cultured cells, whole ventricles of hearts, or hindlimb muscles were subjected to 14% polyacrylamide gel electrophoresis and then transferred to polyvinylidene difluoride membranes. The membranes were then probed with a primary antibody against human decorin, mouse decorin (both from R&D Systems), TGF-β, Smad2, the phosphorylated form of Smad2 (p-Smad2), Smad3, p-Smad3 (all from Cell Signaling), or plasminogen activator inhibitor type 1 (PAI-1; Santa Cruz). Three to five hearts or hindlimb muscles from each group were subjected to the blotting. The blots were visualized using enhanced chemiluminescence (Amersham), and the signals were quantified by densitometry. α-Tubulin (Santa Cruz) served as the loading control.

Electron microscopy. After the hearts were excised, cardiac tissue was quickly cut into 1-mm cubes, immersion fixed in 2.5% glutaraldehyde in 0.1 mol/l phosphate buffer (pH 7.4) overnight at 4°C, and postfixed in 1% buffered osmium tetroxide. The specimens were then dehydrated through a graded ethanol series and embedded in epoxy resin. Ultrathin sections (90 nm), double-stained with uranyl acetate and lead citrate, were examined under an electron microscope (H-800, Hitachi).

Statistical analysis. Values are shown as means ± SE. Survival was analyzed using the Kaplan-Meier method with the log-rank Cox-Mantel method. The significance of differences was evaluated using *t*-tests or one-way ANOVA followed by the Newman-Keul's multiple-comparison test. Values of $P < 0.05$ were considered significant.

RESULTS

Expression of human decorin in vitro and in vivo. Human decorin was strongly expressed on Hela cells transfected with the human decorin gene (Fig. 1, *A* and *B*). In MI mice administered the gene via intramuscular injection into hindlimbs, human decorin was expressed not only in hindlimb muscles, but also in hearts 1 wk after administration (Fig. 1*C*), indicating that the gene product reached the hearts. However, we failed in immunohistochemical detection of human decorin in the heart (photographs not shown), suggesting that the amount of decorin fixed in the cardiac tissue was too small to be detected by the immunohistochemical assay, and that the decorin protein detected by Western blots was mostly the circulating one within the heart. Four weeks later, the expression was markedly reduced but still detectable in both the hindlimb muscles and hearts. No human decorin was detected in the LacZ-treated (control) mice at any time.

Effect of decorin gene treatment on MI at the chronic stage. Within 10 days after induction of MI, six (34%) of the controls and five (31%) of the decorin-treated mice had died. The remaining mice all survived to the end of the observation period (4 wk post-MI). In total, the survival rate was 66% in

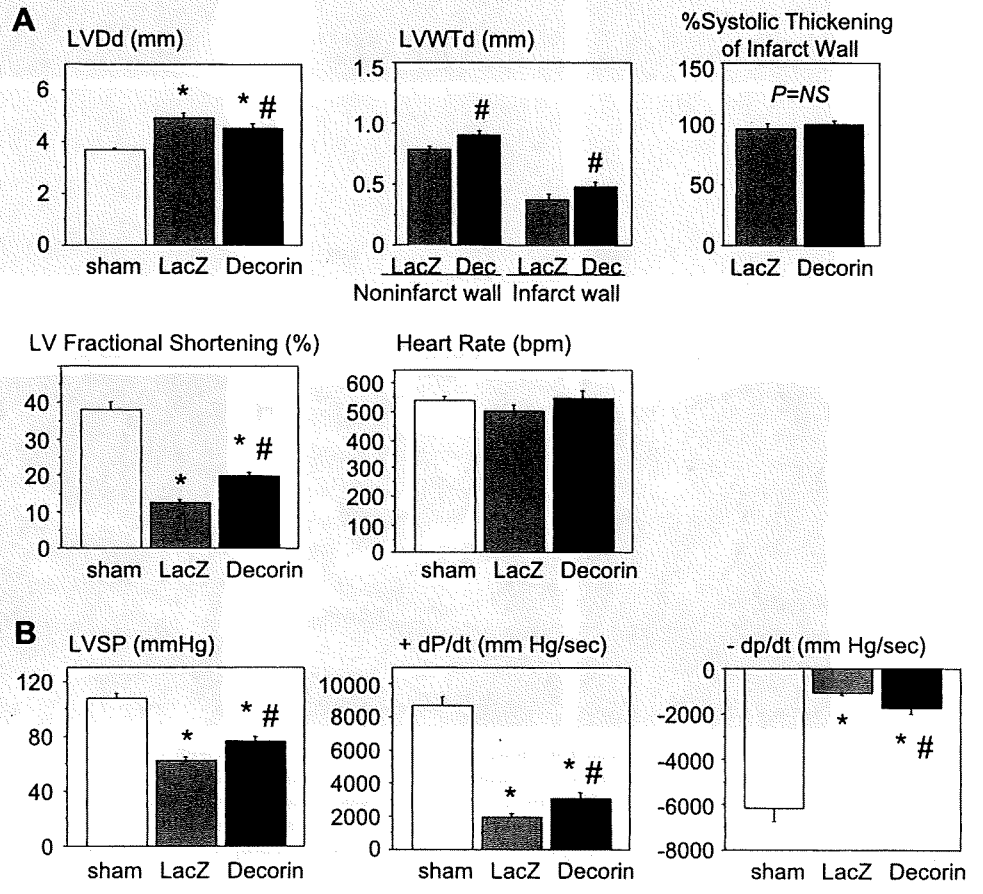

Fig. 2. Left ventricular (LV) geometry and function at the chronic stage (4 wk post-MI) in mice receiving decorin or LacZ gene on *day 3* after MI. *A*: echocardiographic data. *B*: cardiac catheterization data. LVDd, LV end-diastolic diameter; LVWTd, left ventricular wall thickness at diastole; LVSP, LV peak systolic pressure; dP/d*t*, change in pressure over time; NS, nonsignificant; bpm, beats/min. Values are means ± SE. *$P <$ 0.05 vs. sham-operated mice; #$P < 0.05$ vs. LacZ-treated MI mice.

the control group and 69% in the decorin-treated group 4 wk post-MI (P = nonsignificant).

Echocardiography and cardiac catheterization carried out 4 wk post-MI revealed that, compared with the sham-operated mice, control MI mice had marked enlargement of the LV cavity and reduced cardiac function, as indicated by increased LV end-diastolic diameter, increased diastolic thickness of both noninfarct and infarct walls, reduced LV percent fractional shortening, increased LV peak systolic pressure, and increased change in pressure over time (Fig. 2). All of these structural and functional parameters were attenuated in decorin-treated mice, suggesting decorin in some way mitigates post-MI remodeling and cardiac dysfunction. However, the systolic thickening of infarct wall was not increased by the decorin treatment (Fig. 2).

Hearts from control mice showed marked LV dilatation with a thin infarcted segment, while those from decorin-treated mice showed substantially smaller LV cavities and thicker infarcted segments, with shorter circumferential lengths (Fig. 3*A* and Table 1). On the other hand, both the absolute area of the infarct and the percentage of the LV taken up by the infarct were comparable between the two groups (Table 1).

By 4 wk post-MI, the infarct area had been replaced by fibrous scar tissue in the control mice (Fig. 3*B*). In the decorin-treated mice, by contrast, not only collagen fibers but also abundant cellular components were present. As a result, the population of noncardiomyocyte interstitial cells within the infarct area was significantly greater, and the percentage of fibrotic tissue was significantly smaller in decorin-treated mice (Table 1). The number of vWF-positive blood vessels within the infarct area and the percent area of extravascular α-SMA-positive cells were also greater in decorin-treated mice than control mice (Fig. 3, *C* and *D*, and Table 1). On the other hand, there was no significant difference in the populations of CD45-

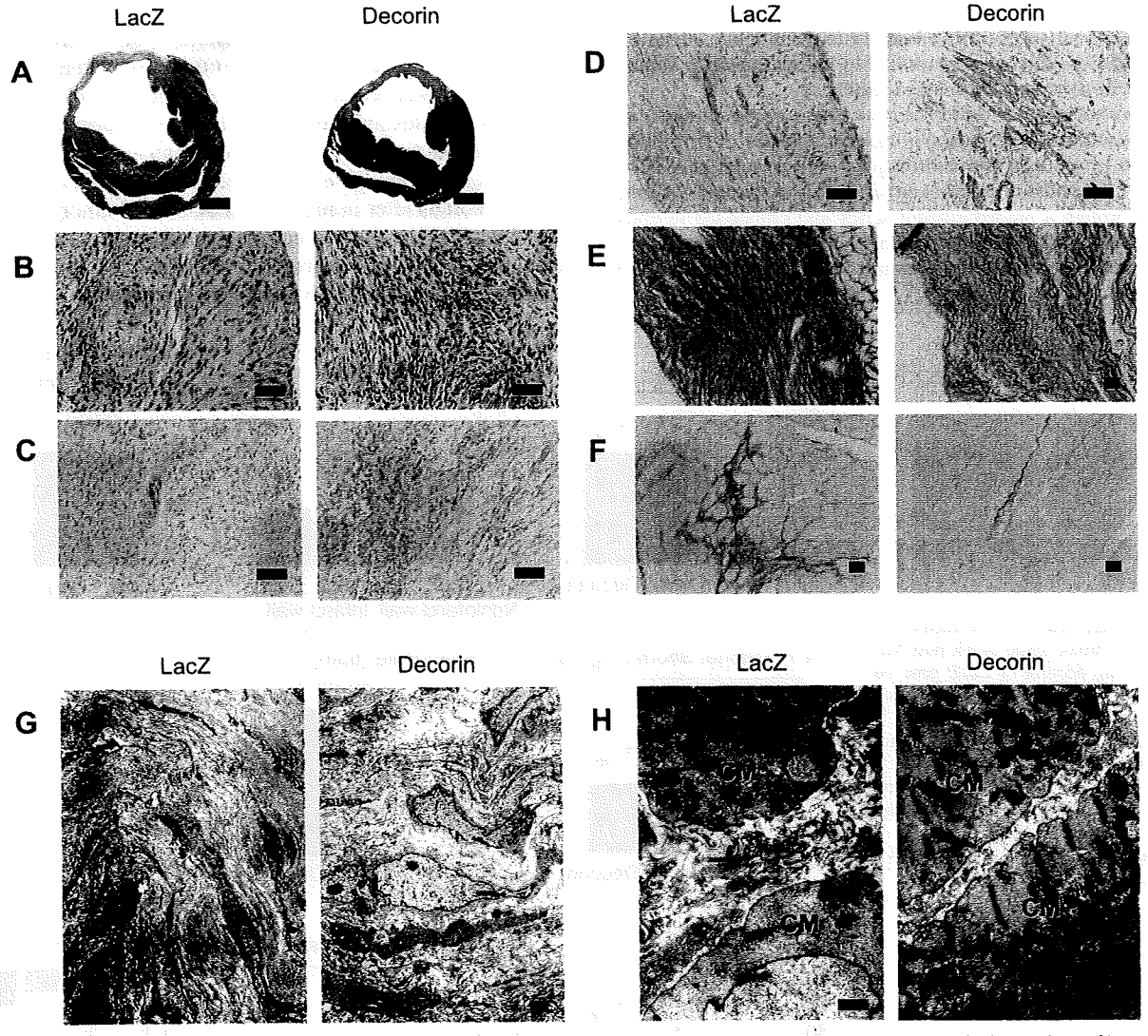

Fig. 3. Gross morphology, histology, immunohistochemistry, and ultrastructure of hearts with 4-wk-old MIs. *A*: transverse ventricular sections of hearts collected from LacZ- and decorin-treated mice. Sections were stained with Masson's trichrome. Note the smaller LV cavity, shorter infarct segments, and thicker infarct walls in the decorin-treated heart. Scale bars, 1 mm. *B–E*: infarcted areas in hearts stained with Masson's trichrome (*B*), anti-von Willebrand factor (vWF; *C*), anti-α-smooth muscle actin (α-SMA; *D*), or Sirius red (*E*). *F*: noninfarcted areas stained with Sirius red. Scale bars, 20 μm. *G* and *H*: electron photomicrographs of collagen fibrils in the infarcted (*G*) and noninfarcted areas (*H*) of the hearts collected from LacZ- and decorin-treated mice. CM, cardiomyocyte. Scale bars, 1 μm.

Table 1. *Effects of treatment with the indicated gene on the morphometry and histology of hearts bearing 4-wk-old MI*

	LacZ	Decorin
n	12	11
Infarcted area		
MI wall thickness, $\times 10^2$ μm	2.9±0.4	4.7±0.4*
MI segmental length, mm	14.2±1.1	10.5±0.7*
%MI segment in LV	50.9±3.9	33.6±2.1*
%MI area in LV	29±8.4	26±6.1
Cell population, no./HPF	1,102±105	1,521±133*
vWF$^+$ vessels, no./HPF	4.8±1.4	9.8±1.3*
α-SMA$^+$ area, %	2.7±0.4	5.1±0.7*
CD45$^+$ leukocytes, no./HPF	2.3±0.3	2.4±0.5
%Fibrosis	62±1.3	51±2.9*
Noninfarcted area		
Myocyte size, μm	17.6±0.8	15.0±0.7*
%Fibrosis	7.1±0.5	4.4±0.5*

Values are means ± SE; *n*, no. of mice. MI, myocardial infarction; LV, left ventricular; HPF, high-power field; α-SMA, α-smooth muscle actin; vWF, von Willebrand factor. *$P < 0.05$ vs. LacZ-treated MI mice.

positive leukocytes between the control and decorin-treated hearts (Table 1). Sirius red staining revealed significantly less fibrosis in both the infracted and noninfarcted LV walls of the decorin-treated mice than the control mice (Fig. 3, *E* and *F*, and Table 1). In addition, the transverse diameter of the cardiomyocytes in the noninfarcted area was significantly greater in the control group than in the decorin-treated group (Table 1), suggesting that compensatory hypertrophy of cardiomyocytes was less developed in the latter. Finally, electron microscopic examination confirmed that collagen fibrils were less developed and scantier in both the infarcted and noninfarcted areas of decorin-treated hearts than control hearts 4 wk post-MI (Fig. 3, *G* and *H*).

Subacute stage of MI. As mentioned above, we observed greater numbers of cells, especially α-SMA-positive myofibroblasts and vWF-positive endothelial cells (in blood vessels), within the infarcted areas of decorin-treated hearts during the chronic stage of MI (4 wk post-MI). To clarify the mechanisms responsible for the difference in the composition of infarct tissue during the chronic stage, we next evaluated cell proliferation and apoptosis among granulation tissue cells in the hearts 10 days post-MI (subacute stage), i.e., 1 wk after gene transfection. Immunohistochemical detection of Ki-67 antigen showed that the incidence of Ki-67 positivity was markedly greater in cardiac tissue from decorin-treated mice than in that from control mice (Fig. 4*A*). Double immunofluorescent staining also revealed that decorin treatment significantly enhanced proliferation of both myofibroblasts and endothelial cells (Fig. 4, *B* and *C*). Conversely, the incidence of TUNEL positivity was significantly smaller in the decorin-treated group than in the control group, suggesting decorin treatment reduced the incidence of apoptosis among granulation tissue cells (Fig. 5*A*). According to Western blot analysis, the cleaved (active) form of caspase-3 was detected, not in the sham-operated mouse hearts, but in the hearts with 10-day-old MI. However, the signal was apparently attenuated in the hearts treated with the decorin

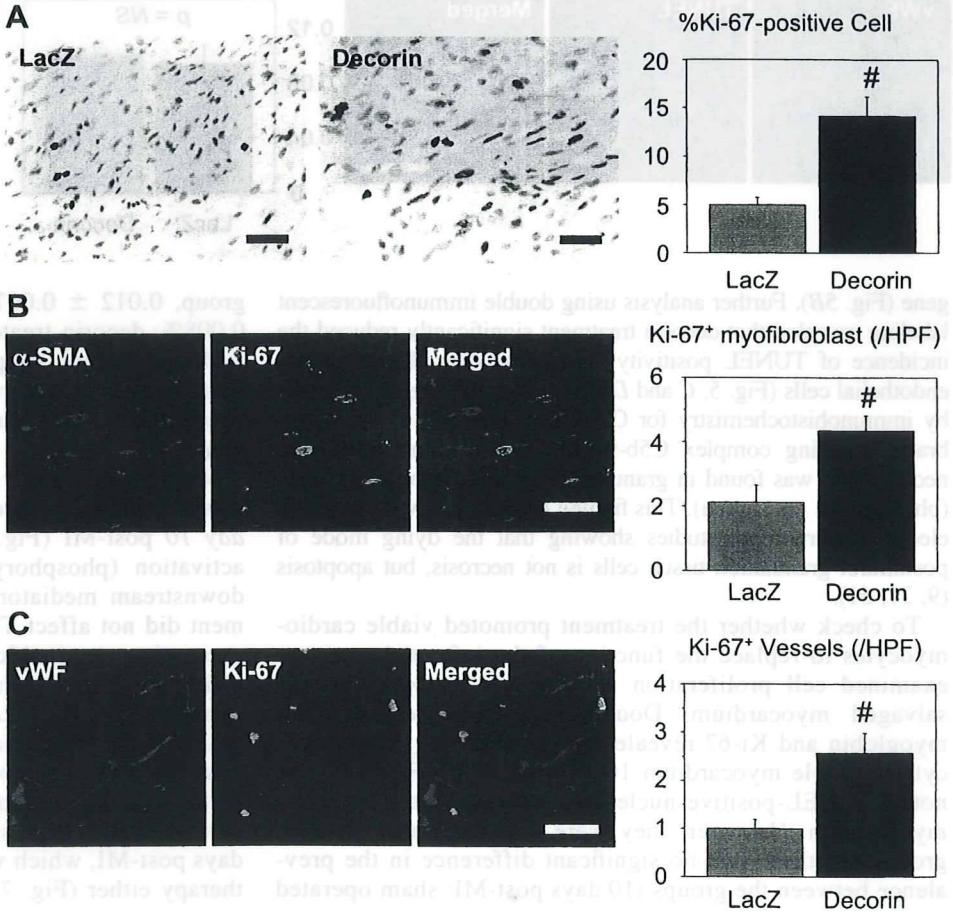

Fig. 4. Cell proliferation within granulation tissue 10 days post-MI. *A*: photomicrographs showing Ki-67-positive cells (*left*) and a graph comparing the incidences of proliferating cells in each group (*right*). *B* and *C*, *left*: confocal photomicrographs of tissue sections from a decorin-treated heart immunolabeled with antibodies against Ki-67 (green fluorescence) plus α-SMA (*B*) or vWF (*C*) (red fluorescence). Scale bars, 20 μm. *Right*: graphs showing the incidences of Ki-67 positivity separately evaluated in myofibroblasts and endothelial cells. HPF, high-powered field. Values in graphs are means ± SE. #$P < 0.05$ vs. LacZ-treated MI mice.

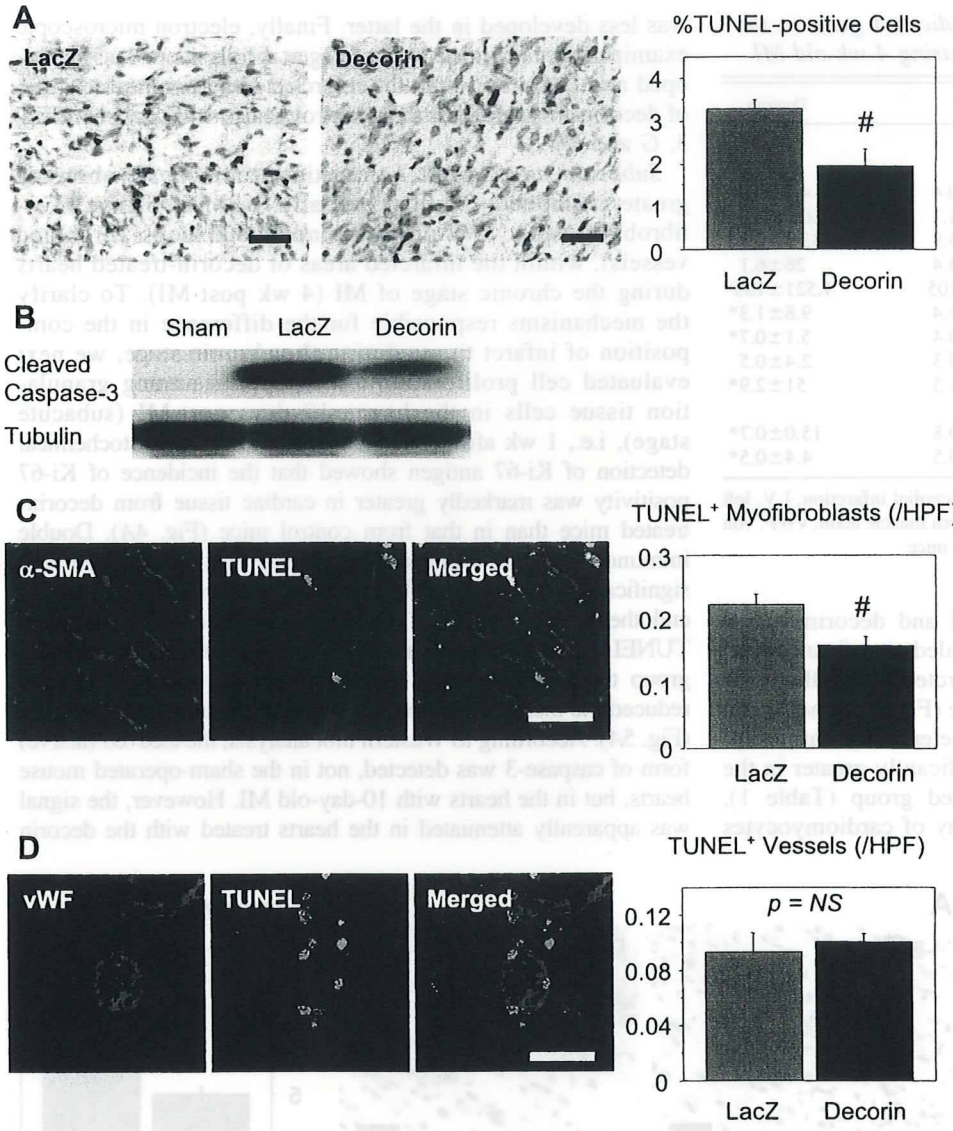

Fig. 5. Apoptosis within granulation tissue 10 days post-MI. *A*: photomicrographs showing terminal deoxynucleotidyl transferase-mediated in situ nick-end labeling (TUNEL)-positive cells (*left*) with a graph comparing the incidences of TUNEL positivity in each group (*right*). *B*: Western blot for the cleaved (activated) caspase-3. *C* and *D*, *left*: confocal photomicrographs of tissue sections from a LacZ-treated heart subjected to TUNEL (green fluorescence) and immunolabeled with antibody against α-SMA (*C*) or vWF (*D*) (red fluorescence). Scale bars, 20 μm. *Right*: graphs showing the incidences of TUNEL positivity separately evaluated in myofibroblasts and endothelial cells. Bars in graphs are means ± SE. #$P <$ 0.05 vs. LacZ-treated MI mice.

gene (Fig. 5*B*). Further analysis using double immunofluorescent labeling revealed that decorin treatment significantly reduced the incidence of TUNEL positivity among myofibroblasts, but not endothelial cells (Fig. 5, *C* and *D*). Next, we investigated necrosis by immunohistochemistry for C9, which is a part of the membrane attacking complex C5b-9 (11). No C9-immunopositive necrotic cell was found in granulation tissue cells of any groups (photographs not shown). This finding is consistent with previous electron microscopic studies showing that the dying mode of postinfarct granulation tissue cells is not necrosis, but apoptosis (9, 37, 51).

To check whether the treatment promoted viable cardiomyocytes to replace the function of the infarcted area, we examined cell proliferation activity and apoptosis in the salvaged myocardium. Double immunofluorescence for myoglobin and Ki-67 revealed no proliferating cardiomyocyte in viable myocardium 10 days post-MI (Fig. 6*A*). We noted TUNEL-positive nuclei of cardiomyocytes in viable myocardium. However, they were extremely rare in each group, and there was no significant difference in the prevalence between the groups (10 days post-MI: sham operated group, 0.012 ± 0.007%; LacZ-treated MI group, 0.010 ± 0.008%; decorin-treated MI group, 0.013 ± 0.011%). These findings do not support the possibility that the present treatments increased regeneration or reduced cell loss due to apoptosis of viable cardiomyocytes to replace the infarcted area.

Western blot analysis showed that expression of TGF-β was significantly upregulated in heart tissues collected on *day 10* post-MI (Fig. 7). Moreover, we observed marked activation (phosphorylation) of Smad2 and Smad3, two downstream mediators of TGF-β. Although decorin treatment did not affect TGF-β or endogenous (mouse) decorin expression, it significantly suppressed Smad2 and Smad3 activation (Fig. 7), which implies that inhibition of signaling in the TGF-β/Smad2/Smad3 pathway contributes substantially to the beneficial effects exerted by decorin against post-MI cardiac remodeling and heart failure. PAI-1 is one of the other important team players in fibrosis (56). Myocardial PAI-1 expression was unchanged in the heart 10 days post-MI, which was not influenced by the decorin gene therapy either (Fig. 7).

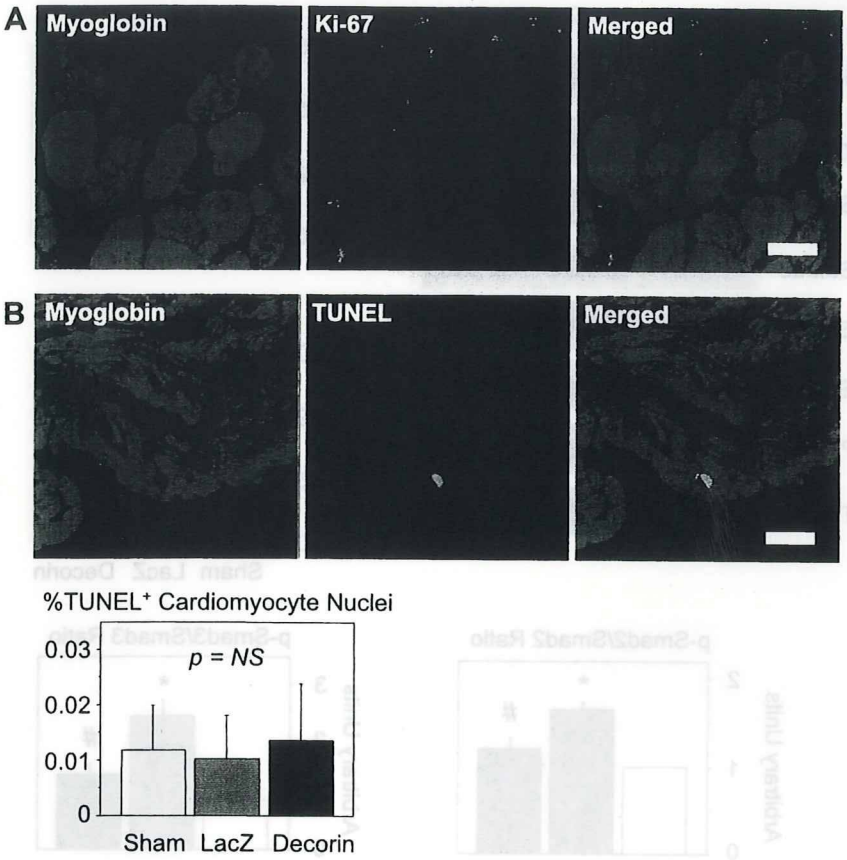

Fig. 6. Cell proliferation and TUNEL positivity of the salvaged cardiomyocytes 10 days post-MI. *A*: confocal photomicrographs of tissue sections from a decorin-treated heart subjected to double immunofluorescence for Ki-67 (green fluorescence) and myoglobin (red fluorescence). There was no Ki-67-positive cardiomyocyte on the preparation where some Ki-67-positive granulation tissue cells or interstitial cells were noted. *B*: confocal photomicrographs of tissue sections from a LacZ-treated heart subjected to double immunofluorescence for TUNEL (green fluorescence) and myoglobin (red fluorescence). TUNEL-positive nuclei of cardiomyocytes were noted, although very rarely. Graph shows the incidences of TUNEL-positive nuclei in cardiomyocytes. Scale bars, 20 μm. Values in graphs are means ± SE.

DISCUSSION

Our findings provide the first evidence that postinfarction decorin gene therapy, started on *day 3* post-MI, mitigates the adverse effects on LV geometry and function during the chronic stage.

Pathophysiological mechanisms for the beneficial effects of decorin gene therapy on postinfarction heart failure. One remarkable finding of the present study is that decorin alters the geometry of the infarct scar without affecting its absolute area, i.e., the infarcted segment was thicker and had a smaller circumferential length in decorin-treated hearts during the chronic stage than in control hearts. This is noteworthy because wall stress is directly proportional to cavity diameter and inversely proportional to wall thickness (Laplace's law) (55) and because wall stress and LV remodeling (dilatation) have a vicious relationship and exacerbate one another. It is thus conceivable that the observed change in infarct geometry would greatly improve the hemodynamic state of the heart.

Our findings also suggest that infarct scar tissue is qualitatively altered by treatment with decorin gene. We observed greater numbers of cells, including abundant myofibroblasts and vascular cells, within the infarct scar in decorin-treated hearts. These cells are normally destined to disappear via apoptosis during the natural course of healing after MI (9, 51), but we found that apoptosis was significantly inhibited in decorin-treated hearts during the subacute stage (10 days post-MI). Moreover, decorin gene therapy also significantly increased cardiac proliferation of both myofibroblasts and vascular endothelial cells. These findings have two important implications. First, both diminished apoptosis and enhanced proliferation among granulation tissue cells during the subacute stage appear to contribute to the observed increase in the cell population within the scar tissue during the chronic stage, which likely preserves the infarct wall thickness. Second, myofibroblasts, which are known to play an important role in wound contraction during the healing process (12), could mediate contraction-induced reduction in the length of the infarct segment, thereby increasing infarct wall thickness. That, in turn, would alter the infarct tissue geometry, reducing wall stress and mitigating LV dilatation and dysfunction.

Vascular endothelial cells also proliferated during the granulation tissue phase in hearts treated with decorin, suggesting an angiogenic effect of decorin. Decorin suppresses malignant tumor cell-mediated angiogenesis (15), whereas it promotes angiogenesis in normal tissue during the healing stage or when ectopically expressed (45, 46). Our finding was well consistent with the latter reports on the role of decorin in angiogenesis. The function of proliferated vascular endothelial cells during the chronic stage of MI remains unclear, although it has been shown that, by supplying blood, newly formed vessels help sustain the cellular components within the infarct area (50). Recently, we reported that blood flow into the infarct area by late reperfusion promotes proliferation and inhibits apoptosis among granulation tissue cells (35). On the other hand, leukocytes continued to die. We suggest that leukocytes may have a higher sensitivity to apoptotic stimuli than other preserved cells, because inflammatory cells generally show very active

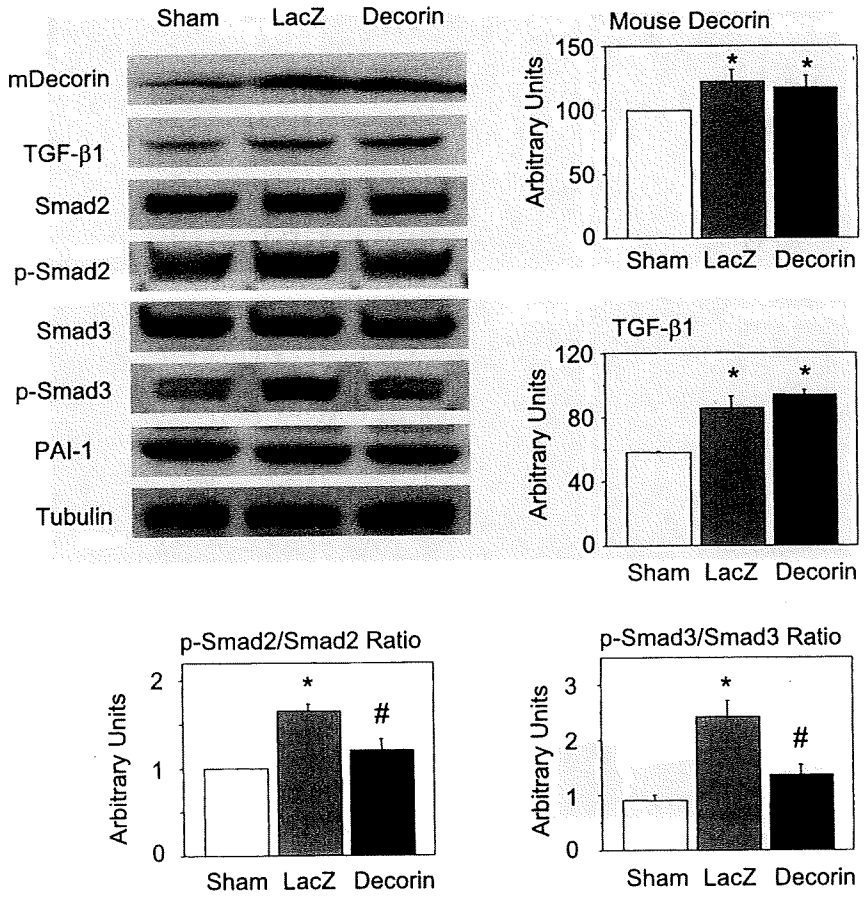

Fig. 7. Western blot analysis for endogeous mouse decorin, transforming growth factor (TGF)-β1, Smad2, Smad3, the phosphorylated (activated) forms of Smad2 (p-Smad2) and Smad3 (p-Smad3), and plasminogen activator inhibitor type 1 (PAI-1) in hearts 10 days post-MI. Graphs show the morphometric data. Values are means ± SE. *$P < 0.05$ vs. sham-operated mice; #$P < 0.05$ vs. LacZ-treated MI mice.

proapoptotic interactions through death ligands and receptors (34).

We also observed that decorin gene therapy significantly reduces cardiac fibrosis, confirming the previously reported antifibrotic effect of decorin in hearts (21). Because myocardial fibrosis contributes to both systolic and diastolic dysfunction (5, 22), its reduction is likely another important way in which decorin may mitigate LV remodeling and heart failure.

In contrast to granulation tissue cells, TUNEL positivity in salvaged cardiomyocytes was not affected by the decorin gene therapy, suggesting no contribution of cardiomyocyte death via apoptosis to the beneficial effects of the therapy. The prevalence of TUNEL-positive cardiomyocyte nuclei was very rare (~0.01%). Although the value is consistent with the previous reports, including ours (38, 44), the discrepancy of the values reported is surprisingly great, ranging from 0.02 to 12% among the studies using mouse model of subacute to chronic stage MI: maximally 600-fold difference (38, 44, 49). It may be problematic that such a critical discrepancy in the TUNEL-positive cardiomyocyte rates remains not yet reconciled, the reason of which should be elucidated in the future.

Ki-67-positive nuclei were not immunohistochemically detected in cardiomyocytes under the present staining conditions. However, immunohistochemical negativity does not always deny the slight expression of an antigen, because the sensitivity depends on the staining conditions. On the other hand, too much sensitivity may violate specificity. Beltrami et al. (2) previously reported cardiomyocyte proliferation by immunohistochemistry in human hearts with MI. It is possible that our immunostaining method for Ki-67 is relatively less sensitive compared with that of the previous report. Notwithstanding, we did detect Ki-67 expression in the granulation tissue cells on the same immunohistochemical preparations, suggesting that our immunohistochemistry was not too insensitive. Difference in immunohistochemical sensitivity and difference in species might have yielded the discrepancy between the studies. The infarct wall did not show a significant systolic thickening, even in the decorin-treated groups, unlikely supporting a possible increase of cardiomyocyte population through increased regeneration and/or reduced apoptosis by the treatment.

Molecular mechanisms involved in the beneficial effects of decorin gene therapy. TGF-β signaling controls a diverse set of cellular processes, including cell apoptosis, differentiation, and proliferation (19, 23, 48). It has also been suggested that TGF-β signaling has both proapoptotic and profibrotic effects on the heart (29, 37). SMAD proteins are important downstream mediators of TGF-β signaling (8, 18), and their absence reportedly impairs local inflammatory responses and accelerates wound healing (1). The most recent findings indicate that loss of Smad3 (in Smad3-null mice) significantly increases myofibroblast density in healing infarcts and prevents myocardial fibrosis (4). In the present study, we observed that cardiac expression of TGF-β, p-Smad2, and p-Smad3 was strongly upregulated in control mice during the granulation tissue phase, 10 days post-MI. Notably, mice receiving the decorin gene expressed high levels of human decorin in the heart 10 days post-MI. Although decorin treatment had no effect on TGF-β expression, it largely blocked the activation of Smad2

and Smad3. This finding, together with those of the aforementioned studies by others, suggests that inhibition of the TGF-β/Smad2/Smad3 pathway contributes substantially to the reduction in cardiac fibrosis, as well as the reduced apoptosis and increased proliferation seen among granulation tissue cells in decorin-treated mice. Collectively, these effects would be expected to alter infarct tissue geometry to reduce wall stress and suppress myocardial fibrosis, thereby mitigating post-MI cardiac remodeling and dysfunction.

Hao et al. (17) previously reported increased protein expression levels of Smad2 and 3 in the rat MI model, which may appear to be inconsistent with our results that revealed activation of Smad2 and Smad3, but not upregulation of them. The most important difference may be the timing of examination, as well as difference in species (rat vs. mouse), which caused apparent conflict between the studies; Hao et al. examined MI at 8 wk after the onset, while we used 10-day-old MI. Hao et al. actually found that endogenous decorin expression was stronger in the hearts with older infarction.

It was not unexpected that the decorin gene therapy showed beneficial effects on postinfarction hearts in a strikingly similar manner as the previously reported sTβRII gene therapy, because decorin is a natural inhibitor of TGF-β, while sTβRII competitively inhibits binding of TGF-β with the TGF-β receptor (37). Pathophysiological mechanisms were very similar between these two gene therapies, as discussed above. In the present study, however, we found that decorin could increase cell proliferation in postinfarction granulation tissue and elucidated the inhibitory effect of decorin on TGF-β downstream signaling activation.

Possible clinical implications and limitations. Rapid recanalization of the occluded coronary artery, which salvages ischemic myocardial cells, is the best clinical approach at present to treating acute MI. Unfortunately, most patients actually lose their chance for coronary reperfusion therapy because it is only effective if performed within hours after the onset of infarction (41). The present findings suggest a novel therapeutic strategy, applicable during the subacute stage of MI, that may mitigate chronic progressive heart failure in MI patients who missed their chance for coronary reperfusion during the acute stage. In addition, treatment with decorin may be more promising than the use of sTβRII, which simply inhibits TGF-β signaling, when considering its additive beneficial effects, such as anti-tumor metastasis actions (15, 40, 52).

However, safety of anti-decorin strategies has not been confirmed in humans. In addition, ethical consensus has not been established at all in the safety of a virus-mediated gene therapy. These issues should be resolved before clinical application of the anti-decorin gene therapy.

ACKNOWLEDGMENTS

We thank Hatsue Ohshika in Gifu University Graduate School of Medicine for technical assistance.

GRANTS

This study was supported, in part, by postdoctoral fellowship for foreign researchers (to L. Li), by the Japan Society for the Promotion of Science, and by a Research Grant from Gifu University.

REFERENCES

1. **Ashcroft GS, Yang X, Glick AB, Weinstein M, Letterio JL, Mizel DE, Anzano M, Greenwell-Wild T, Wahl SM, Deng C, Roberts AB.** Mice lacking Smad3 show accelerated wound healing and an impaired local inflammatory response. *Nat Cell Biol* 1: 260–266, 1999.
2. **Beltrami AP, Urbanek K, Kajstura J, Yan SM, Finato N, Bussani R, Nadal-Ginard B, Silvestri F, Leri A, Beltrami CA, Anversa P.** Evidence that human cardiac myocytes divide after myocardial infarction. *N Engl J Med* 344: 1750–1757, 2001.
3. **Bourassa MG, Gurné O, Bangdiwala SI, Ghali JK, Young JB, Rousseau M, Johnstone DE, Yusuf S.** Natural history and patterns of current practice in heart failure. *J Am Coll Cardiol* 22, *Suppl* A: 14A–19A, 1993.
4. **Bujak M, Ren G, Kweon HJ, Dobaczewski M, Reddy A, Taffet G, Wang XF, Frangogiannis NG.** Essential role of Smad3 in infarct healing and in the pathogenesis of cardiac remodeling. *Circulation* 116: 2127–2138, 2007.
5. **Burlew BS, Weber KT.** Connective tissue and the heart: functional significance and regulatory mechanisms. *Cardiol Clin* 18: 435–442, 2000.
6. **Chen SH, Chen XH, Wang Y, Kosai K, Finegold MJ, Rich SS, Woo SL.** Combination gene therapy for liver metastasis of colon carcinoma in vivo. *Proc Natl Acad Sci USA* 92: 2577–2581, 1995.
7. **Cheng W, Kajstura J, Nitahara JA, Li B, Reiss K, Liu Y, Clark WA, Krajewski S, Reed JC, Olivetti G, Anversa P.** Programmed myocyte cell death affects the viable myocardium after infarction in rats. *Exp Cell Res* 226: 316–327, 1996.
8. **Derynck R, Zhang YE.** Smad-dependent and Smad-independent pathways in TGF-beta family signalling. *Nature* 425: 577–584, 2003.
9. **Desmoulière A, Redard M, Darby I, Gabbiani G.** Apoptosis mediates the decrease in cellularity during the transition between granulation tissue and scar. *Am J Pathol* 146: 56–66, 1995.
10. **Deten A, Holzl A, Leicht M, Barth W, Zimmer HG.** Changes in extracellular matrix and in transforming growth factor beta isoforms after coronary artery ligation in rats. *J Mol Cell Cardiol* 33: 1191–1207, 2001.
11. **Doran JP, Howie AJ, Townend JN.** Detection of myocardial infarction by immunohistological staining for C9 on formalin fixed, paraffin wax embedded sections. *J Clin Pathol* 49: 34–37, 1996.
12. **Gabbiani G.** The myofibroblast in wound healing and fibrocontractive diseases. *J Pathol* 200: 500–503, 2003.
13. **Gheorghiade M, Bonow RO.** Chronic heart failure in the United States: a manifestation of coronary artery disease. *Circulation* 97: 282–289, 1998.
14. **Gheorghiade M, Sopko G, De Luca L, Velazquez EJ, Parker JD, Binkley PF, Sadowski Z, Golba KS, Prior DL, Rouleau JL, Bonow RO.** Navigating the crossroads of coronary artery disease and heart failure. *Circulation* 114: 1202–1213, 2006.
15. **Grant DS, Yenisey C, Rose RW, Tootell M, Santra M, Iozzo RV.** Decorin suppresses tumor cell-mediated angiogenesis. *Oncogene* 21: 4765–4777, 2002.
16. **Hamner JB, Ellison KJ.** Predictors of hospital readmission after discharge in patients with congestive heart failure. *Heart Lung* 34: 231–239, 2005.
17. **Hao J, Ju H, Zhao S, Junaid A, Scammell-La Fleur T, Dixon IM.** Elevation of expression of Smad2, 3, and 4, decorin and TGF-beta in the chronic phase of myocardial infarct scar healing. *J Mol Cell Cardiol* 31: 667–678, 1999.
18. **Heldin CH, Miyazono K, ten Dijke P.** TGF-beta signalling from cell membrane to nucleus through SMAD proteins. *Nature* 390: 465–471, 1997.
19. **Huang SS, Huang JS.** TGF-beta control of cell proliferation. *J Cell Biochem* 96: 447–462, 2005.
20. **Isaka Y, Akagi Y, Ando Y, Tsujie M, Sudo T, Ohno N, Border WA, Noble NA, Kaneda Y, Hori M, Imai E.** Gene therapy by transforming growth factor-beta receptor-IgG Fc chimera suppressed extracellular matrix accumulation in experimental glomerulonephritis. *Kidney Int* 55: 465–475, 1999.
21. **Jahanyar J, Joyce DL, Southard RE, Loebe M, Noon GP, Koerner MM, Torre-Amione G, Youker KA.** Decorin-mediated transforming growth factor-beta inhibition ameliorates adverse cardiac remodeling. *J Heart Lung Transplant* 26: 34–40, 2007.
22. **Jalil JE, Doering CW, Janicki JS, Pick R, Shroff SG, Weber KT.** Fibrillar collagen and myocardial stiffness in the intact hypertrophied rat left ventricle. *Circ Res* 64: 1041–1050, 1989.
23. **Jang CW, Chen CH, Chen CC, Chen JY, Su YH, Chen RH.** TGF-beta induces apoptosis through Smad-mediated expression of DAP-kinase. *Nat Cell Biol* 4: 51–58, 2002.
24. **Kaiser J.** Clinical research. Death prompts a review of gene therapy vector. *Science* 317: 580, 2007.

25. **Krusius T, Ruoslahti E.** Primary structure of an extracellular matrix proteoglycan core protein deduced from cloned cDNA. *Proc Natl Acad Sci USA* 83: 7683–7687, 1986.
26. **Levy D, Kenchaiah S, Larson MG, Benjamin EJ, Kupka MJ, Ho KK, Murabito JM, Vasan RS.** Long-term trends in the incidence of and survival with heart failure. *N Engl J Med* 347: 1397–1402, 2002.
27. **Li Y, Takemura G, Kosai K, Takahashi T, Okada H, Miyata S, Yuge K, Nagano S, Esaki M, Khai NC, Goto K, Mikami A, Maruyama R, Minatoguchi S, Fujiwara T, Fujiwara H.** Critical roles for the Fas/Fas ligand system in postinfarction ventricular remodeling and heart failure. *Circ Res* 95: 627–236, 2004.
28. **Li Y, Li J, Zhu J, Sun B, Branca M, Tang Y, Foster W, Xiao X, Huard J.** Decorin gene transfer promotes muscle cell differentiation and muscle regeneration. *Mol Ther* 15: 1616–1622, 2007.
29. **Lijnen PJ, Petrov VV, Fagard RH.** Induction of cardiac fibrosis by transforming growth factor-beta 1. *Mol Genet Metab* 71: 418–435, 2000.
30. **Marshall E.** Gene therapy death prompts review of adenovirus vector. *Science* 286: 2244–2245, 1999.
31. **Masuda H, Takakura Y, Hashida M.** Pharmacokinetics and disposition characteristics of recombinant decorin after intravenous injection into mice. *Biochim Biophys Acta* 1426: 420–428, 1999.
32. **McKay RG, Pfeffer MA, Pasternak RC, Markis JE, Come PC, Nakao S, Alderman JD, Ferguson JJ, Safian RD, Grossman W.** Left ventricular remodeling after myocardial infarction: a corollary to infarct expansion. *Circulation* 74: 693–702, 1986.
33. **Mizuguchi H, Kay MA.** A simple method for constructing E1- and E1/E4-deleted recombinant adenoviral vectors. *Hum Gene Ther* 10: 2013–2017, 1999.
34. **Nagata S.** Apoptosis by death factor. *Cell* 88: 355–365, 1997.
35. **Nakagawa M, Takemura G, Kanamori H, Goto K, Maruyama R, Tsujimoto A, Ohno T, Okada H, Ogino A, Esaki M, Miyata S, Li L, Ushikoshi H, Aoyama T, Kawasaki M, Nagashima K, Fujiwara T, Minatoguchi S, Fujiwara H.** Mechanisms by which late coronary reperfusion mitigates postinfarction cardiac remodeling. *Circ Res* 103: 98–106, 2008.
36. **Ogino A, Takemura G, Kanamori H, Okada H, Maruyama R, Miyata S, Esaki M, Nakagawa M, Aoyama T, Ushikoshi H, Kawasaki M, Minatoguchi S, Fujiwara T, Fujiwara H.** Amlodipine inhibits granulation tissue cell apoptosis through reducing calcineurin activity to attenuate postinfarction cardiac remodeling. *Am J Physiol Heart Circ Physiol* 293: H2271–H2280, 2007.
37. **Okada H, Takemura G, Kosai K, Li Y, Takahashi T, Esaki M, Yuge K, Miyata S, Maruyama R, Mikami A, Minatoguchi S, Fujiwara T, Fujiwara H.** Postinfarction gene therapy against transforming growth factor-beta signal modulates infarct tissue dynamics and attenuates left ventricular remodeling and heart failure. *Circulation* 111: 2430–2437, 2005.
38. **Okada H, Takemura G, Kosai K, Tsujimoto A, Esaki M, Takahashi T, Nagano S, Kanamori H, Miyata S, Li Y, Ohno T, Maruyama R, Ogino A, Li L, Nakagawa M, Nagashima K, Fujiwara T, Fujiwara H, Minatoguchi S.** Combined therapy with cardioprotective cytokine administration and antiapoptotic gene transfer in postinfarction heart failure. *Am J Physiol Heart Circ Physiol* 296: H616–H626, 2009.
39. **Pfeffer MA.** Left ventricular remodeling after acute myocardial infarction. *Annu Rev Med* 46: 455–466, 1995.
40. **Reed CC, Waterhouse A, Kirby S, Kay P, Owens RT, McQuillan DJ, Iozzo RV.** Decorin prevents metastatic spreading of breast cancer. *Oncogene* 24: 1104–1110, 2005.
41. **Reimer KA, Vander Heide RS, Richard VJ.** Reperfusion in acute myocardial infarction: effect of timing and modulating factors in experimental models. *Am J Cardiol* 72: 13G–21G, 1993.
42. **Rissanen TT, Ylä-Herttuala S.** Current status of cardiovascular gene therapy. *Mol Ther* 15: 1233–1247, 2007.
43. **Ruoslahti E.** Structure and biology of proteoglycans. *Annu Rev Cell Biol* 4: 229–255, 1988.
44. **Sam F, Sawyer DB, Xie Z, Chang DL, Ngoy S, Brenner DA, Siwik DA, Singh K, Apstein CS, Colucci WS.** Mice lacking inducible nitric oxide synthase have improved left ventricular contractile function and reduced apoptotic cell death late after myocardial infarction. *Circ Res* 89: 351–356, 2001.
45. **Santra M, Santra S, Zhang J, Chopp M.** Ectopic decorin expression up-regulates VEGF expression in mouse cerebral endothelial cells via activation of the transcription factors Sp1, HIF1alpha, and Stat3. *J Neurochem* 105: 324–337, 2008.
46. **Schönherr E, Sunderkötter C, Schaefer L, Thanos S, Grässel S, Oldberg A, Iozzo RV, Young MF, Kresse H.** Decorin deficiency leads to impaired angiogenesis in injured mouse cornea. *J Vasc Res* 41: 499–508, 2004.
47. **Shan K, Kurrelmeyer K, Seta Y, Wang F, Dibbs Z, Deswal A, Lee-Jackson D, Mann DL.** The role of cytokines in disease progression in heart failure. *Curr Opin Cardiol* 12: 218–223, 1997.
48. **Shi Y, Massagué J.** Mechanisms of TGF-beta signaling from cell membrane to the nucleus. *Cell* 113: 685–700, 2003.
49. **Singla DK, Lyons GE, Kamp TJ.** Transplanted embryonic stem cells following mouse myocardial infarction inhibit apoptosis and cardiac remodeling. *Am J Physiol Heart Circ Physiol* 293: H1308–H1314, 2007.
50. **Sun Y, Weber KT.** Infarct scar: a dynamic tissue. *Cardiovasc Res* 46: 250–256, 2000.
51. **Takemura G, Ohno M, Hayakawa Y, Misao J, Kanoh M, Ohno A, Uno Y, Minatoguchi S, Fujiwara T, Fujiwara H.** Role of apoptosis in the disappearance of infiltrated and proliferated interstitial cells after myocardial infarction. *Circ Res* 82: 1130–1138, 1998.
52. **Tran KT, Lamb P, Deng JS.** Matrikines and matricryptins: implications for cutaneous cancers and skin repair. *J Dermatol Sci* 40: 11–20, 2005.
53. **Weisman HF, Bush DE, Mannisi JA, Weisfeldt ML, Healy B.** Cellular mechanisms of myocardial infarct expansion. *Circulation* 78: 186–201, 1988.
54. **Yamaguchi Y, Mann DM, Ruoslahti E.** Negative regulation of transforming growth factor-beta by the proteoglycan decorin. *Nature* 346: 281–284, 1990.
55. **Yin FC.** Ventricular wall stress. *Circ Res* 49: 829–842, 1981.
56. **Zaman AK, French CJ, Schneider DJ, Sobel BE.** A profibrotic effect of plasminogen activator inhibitor type-1 (PAI-1) in the heart. *Exp Biol Med (Maywood)* 234: 246–254, 2009.

The knock-down of overexpressed EZH2 and BMI-1 does not prevent osteosarcoma growth

HIROMI SASAKI*, TAKAO SETOGUCHI*, YUKIHIRO MATSUNOSHITA, HUI GAO, MASATAKA HIROTSU and SETSURO KOMIYA

[1]Department of Orthopaedic Surgery, Graduate School of Medical and Dental Sciences, Kagoshima University, 8-35-1 Sakuragaoka, Kagoshima 890-8520, Japan

Received September 17, 2009; Accepted October 12, 2009

DOI: 10.3892/or_00000684

Abstract. Polycomb group proteins control the transcriptional memory of cells by maintaining the stable silencing of specific sets of genes through chromatin modifications. Polycomb group protein complexes control gene repression through recruitment of histone deacetylase. This recruitment leads to trimethylation of Lys_{27} of histone H3 (H3K27). Histone H3K27 trimethylation is a property of stably silenced heterochromatin. EZH2 and BMI-1 are pivotal components of polycomb group protein complexes. Increased *EZH2* levels have been found in several malignancies and reported as a molecular biomarker of poor prognosis. Similarly, *BMI-1* has also been found to be associated with malignant transformation. In addition, inhibition of *EZH2* or *BMI-1* inhibits the growth of various types of malignancies. The expression of *BMI-1* and *EZH2* in human osteosarcoma has not been clearly determined. We examined the potential involvement of aberrant polycomb group protein expression in the pathogenesis of osteosarcoma. Real-time PCR revealed that expression of *EZH2* in 143B, HOS, NOS-1 and Saos2 was increased compared to normal osteoblasts. *BMI-1* was also up-regulated in 143B, HOS and NOS-1. Expression of *EZH2* and *BMI-1* were up-regulated in osteosarcoma patient biopsy specimens compared to normal bone. Immunohistochemical examinations showed that EZH2 and BMI-1 were up-regulated in osteosarcoma cells and that trimethylation of histone H3K27 was increased. We examined the effects of knock down of *EZH2* and *BMI-1* by shRNA. Unexpectedly, the knock-down of *EZH2* and *BMI-1* did not prevent osteosarcoma growth either *in vitro* or *in vivo*. Our findings suggest that EZH2 and BMI-1 may be tumor-associated antigens of osteosarcoma, but are not useful molecular targets of osteosarcoma treatment.

Correspondence to: Dr Takao Setoguchi, Department of Orthopaedic Surgery, Graduate School of Medical and Dental Sciences, Kagoshima University, 8-35-1 Sakuragaoka, Kagoshima 890-8520, Japan
E-mail: setoro@m2.kufm.kagoshima-u.ac.jp

*Contributed equally

Key words: polycomb protein, osteosarcoma, EZH2, BMI-1

Introduction

Osteosarcoma is the most common primary bone cancer occurring mainly in children (1). Standard treatment involves the use of 'up-front' multi-agent chemotherapy, definitive surgery of the primary tumor and postoperative chemotherapy. In recent years, great effort has been made aiming at elucidating the molecular events underpinning the biology of osteosarcoma including dysregulation of cell division and apoptotic processes. Although such dysregulation may constitute a potent source of new therapeutic targets, the molecular mechanisms of regulation of osteosarcoma cell proliferation are largely unknown.

Polycomb group (PcG) proteins control the transcriptional memory of cells by maintaining the stable silencing of specific sets of genes through chromatin modifications (2). Two distinct and evolutionarily conserved PcG complexes have been identified, consisting of various PcG proteins and non-PcG proteins. The polycomb repressive complex 1 (PRC1) contains the BMI-1, MEL-18, RING1, HPH and HPC PcG proteins, while the polycomb repressive complex 2 (PRC2) contains the EZH2, EED, YY1 and SUZ PcG proteins (3-15). EZH2 is a histone methyltransferase associated with transcriptional repression. EZH2 catalyzes trimethylation of histone H3 at lysine 27 (H3K27) (16-19).

Recent findings have linked deregulated expression of human PcG genes to malignant transformation, loss of differentiation in tumor cells, and metastatic behavior (20). Increased *EZH2* levels have been found in several epithelial tumors (21-26) and in various hematological malignancies (27-29). Similarly, *BMI-1* has also been associated with malignant transformation (23,27,30-38). The expression of *BMI-1* and *EZH2* in human osteosarcoma cell lines and osteosarcoma patient specimens have not been well defined. To explore the potential involvement of aberrant PcG expression in the pathogenesis of osteosarcoma, we investigated the expression of *EZH2* and *BMI-1* in osteosarcoma cell lines and patient samples. We next examined the status of trimethylation of H3K27. In addition, we examined the effect of the knock-down of *EZH2* and *BMI-1* by shRNA *in vitro* and *in vivo*.

Materials and methods

Cell culture. HOS, 143B and Saos2 cells were purchased from the American Type Culture Collection (ATCC). NOS-1 was purchased from RIKEN cell bank (39). Cells were grown in Dulbecco's modified Eagle's medium (DMEM) supplemented with 10% FBS, penicillin (100 U/ml) and streptomycin (100 μg/ml). Human osteoblast cells (NHOst) were purchased from Sanko Junyaku (Tokyo, Japan). Cells were cultured with OBM™ (Cambrex, NJ, USA) or DMEM supplemented with 10% FBS. All cells were grown in a humidified atmosphere containing 5% CO_2 at 37˚C.

Patient osteosarcoma biopsy specimens. All human osteosarcoma biopsy specimens were obtained from primary lesions. Biopsy was performed before chemotherapy or radio therapy to make the diagnosis.

RT-PCR. Each sample was run minimally at three concentrations in triplicate. All primer sets amplified 100- to 200-bp fragments. Total RNA was extracted using the miR-Vana RNA isolation system (Ambion, TX, USA) or TRIzol (Invitrogen, CA, USA). Reactions were run using SYBR-Green (Bio-Rad, CA, USA) on a MiniOpticon™ machine (Bio-Rad). The comparative Ct ($\Delta\Delta$Ct) method was used to determine fold change in expression using ßII-microglobulin. Each sample was run minimally at three concentrations in triplicate. The following primers were used. EZH2: 5-TTCA TGCAACACCCAACACT-3, 5-GAGAGCAGCAGCAAAC TCCT-3; BMI-1: 5-TTCATTGATGCCACAACCAT-3, 5-GTA CTGGGGCTAGGCAAACA; ßII-microglobulin: 5-TCAATG TCGGATGGATGAAA-3, 5-GTGCTCGCGCTACTCTC TCT-3.

Cell proliferation assay. MTT assay: Cells were incubated with substrate with MTT [3-(4,5-dimethylthiazol-2-yl)-2,5-diphenyltetrazolium bromide] for 4 h and washed with PBS and lysed to release formazan from cells. Then cells were analyzed in a Safire microplate reader (Bio-Rad) at 562 nm. shRNAs were purchased from (SABiosciences, MD, USA). Lipofection of siRNA was performed every other day as recommended in the supplier's protocol using FuGENE 6 (Roche, Basel, Switzerland).

Immunohistochemistry. The following primary antibodies were used: anti-EZH2 (diluted 1:200 Zymed Laboratories, CA, USA), anti-BMI-1 (diluted 1:200 R&D Systems, MN, USA), and anti-trimethylated H3K27 (diluted 1:200 Abcam, Cambridge, UK). The following secondary antibodies were used: fluorescein-conjugated goat anti-mouse IgG antibody (diluted 1:200; Jackson ImmunoResearch, PA, USA) and rhodamine-conjugated donkey anti-rabbit IgG antibody (diluted 1:200; Chemicon, CA, USA). The cells were counterstained with Hoechst 33258 to identify nuclei. Immunohistochemistry with each second antibody alone without primary antibody was performed as a control.

Animal experiments. shRNA-transfected 143B cells ($1x10^5$) were mixed with collagen gel in a 1:1 volume and inoculated subcutaneously in 5-week-old nude mice. Tumor size was measured, and tumor volume was calculated using the formula $LW^2/2$ (with L and W representing the length and width of tumors). All experimental procedures were performed in compliance with the guiding principles for the Care and Use of Animals described in the American Journal of Physiology and with the Guidelines established by the Institute of Laboratory Animal Sciences, Faculty of Medicine, Kagoshima University. All efforts were made to minimize animal suffering, to reduce the number of animals used and to utilize possible alternatives to *in vivo* techniques.

Data analysis. Each sample was analyzed in triplicate and experiments were repeated three times. In figures the error bar means standard error. Data were analyzed by the STASTISCA (StatSoft, OK, USA). Differences between mean values were evaluated by the unpaired t-test and differences in frequencies were evaluated by Fisher's exact test. Results were considered statistically significant at $P<0.05$.

Results

Overexpression of EZH2 and BMI-1 in osteosarcoma. RT-PCR was performed to examine the expression of *EZH2* and *BMI-1* in osteosarcoma cell lines. RT-PCR revealed that NOS-1, HOS and 143B osteosarcoma cell lines expressed EZH2 more strongly than normal human osteoblasts (NHOst) (Fig. 1A). More sensitive real-time PCR analyses revealed that expression of *EZH2* in 143B, HOS, NOS-1 and Saos2 was increased 13-, 11-, 4.9- and 4.4-fold, respectively (Fig. 1B). RT-PCR revealed that NOS-1, HOS and 143B osteosarcoma cell lines expressed *BMI-1* more strongly than NHOst (Fig. 1C). Real-time PCR revealed that expression of *BMI-1* in 143B, HOS and NOS-1 was increased 6.7-, 3.7- and 3.7-fold, respectively, while that in Saos2 did not change appreciably (Fig. 1D). We next examined the expression of *EZH2* and *BMI-1* in osteosarcoma patient biopsy samples. RT-PCR revealed that 3 osteosarcoma patient samples expressed EZH2 more strongly than normal bone tissue (Fig. 1E). Real-time PCR revealed that expression of *EZH2* in patient samples was increased 1.4- to 4.2-fold (Fig. 1F). RT-PCR revealed that 3 osteosarcoma patient samples expressed *BMI-1* more strongly than normal bone (Fig. 1G). Real-time PCR revealed that expression of *BMI-1* in patient samples increased 4.5- to 9.4-fold (Fig. 1H). To extend these findings, we performed immunohistochemistry for EZH2 and BMI-1 examination revealed that osteosarcoma cell lines and osteosarcoma patient samples expressed EZH2 and BMI-1 more strongly than normal bone tissue (Fig. 2A and B). EZH2 and BMI-1 were localized in the nucleus of osteosarcoma cells (Fig. 2A and B). These findings showed that EZH2 and BMI-1 are overexpressed in osteosarcomas.

Histone H3-K27 is trimethylated in osteosarcoma. To determine if overexpression of polycomb proteins promoted histone H3K27 trimethylation, we performed immunohistochemical examination using trimethylated histone H3K27-specific antibody. Histone H3K27 was found to be trimethylated more strongly in osteosarcoma cells lines and osteosarcoma patient samples than in normal osteoblasts and bone tissue (Fig. 2C).

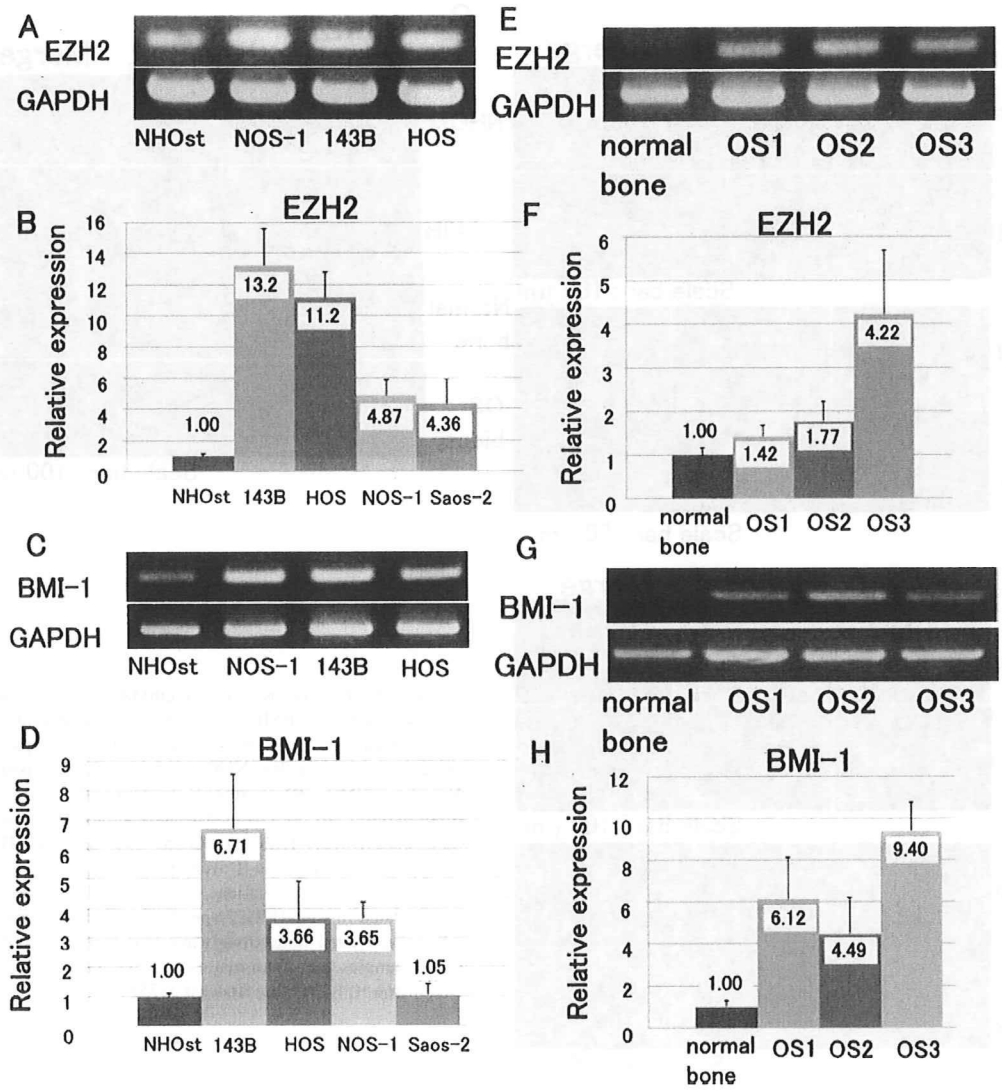

Figure 1. Overexpression of *EZH2* and *BMI-1* in osteosarcoma. (A) RT-PCR revealed that 3 osteosarcoma cell lines including NOS-1, 143B and HOS expressed *EZH2* more strongly than NHOst (normal osteoblasts). (B) Real-time PCR revealed that expression of *EZH2* in 143B, HOS, NOS-1 and Saos2 was increased 13-, 11-, 4.9- and 4.4-fold, respectively. (C) RT-PCR revealed that 3 osteosarcoma cell lines including NOS-1, 143B and HOS expressed *BMI-1* more strongly than NHOst. (D) Real-time PCR revealed that expression of *BMI-1* in 143B, HOS and NOS-1 was increased 6.7-, 3.7- and 3.7-fold, respectively, while that in Saos2 did not change appreciably. (E) Total RNA extracted from osteosarcoma biopsy samples were used for RT-PCR. RT-PCR revealed that osteosarcoma biopsy sample 1 (OS1), OS2 and OS3 expressed *EZH2* more strongly than normal bone. (F) Real-time PCR revealed that expression of *EZH2* in patient samples was increased 1.2- to 4.2-fold. (G) RT-PCR revealed that 3 osteosarcoma samples expressed *BMI-1* more strongly than normal bone. (H) Real time PCR revealed that expression of *BMI-1* in patient samples increased 4.5 to 9.4 fold.

Knock-down of overexpressed EZH2 and BMI-1 does not prevent osteosarcoma growth in vitro or in vivo. It has been reported that overexpression of EZH2 or BMI-1 promotes malignant transformation (21,36,38,40-47). In addition, inhibition of EZH2 or BMI-1 inhibits growth of various types of malignancies (38,41,43,45,46). To determine whether knock-down of *EZH2* and *BMI-1* prevents osteosarcoma growth, we examined the effects of *EZH2* and *BMI-1* shRNA. We used 143B and HOS, which strongly express EZH2 and BMI-1. Real-time PCR revealed that shRNA effectively knocked-down *EZH2* and *BMI-1* (Fig. 3A). 143B and HOS were transfected with *EZH2* shRNA, *BMI-1* shRNA and *EZH2* shRNA plus *BMI-1* shRNA. Unexpectedly, MTT assay revealed that the knock-down of *EZH2*, *BMI-1* and *EZH2* plus *BMI-1* did not prevent osteosarcoma growth *in vitro* (Fig. 3B-D). To confirm the effects of *EZH2* and *BMI-1* knock-down, we examined xenograft models. Nude mice were inoculated with control shRNA-transfected 143B cells, *EZH2* shRNA-transfected 143B cells and *BMI-1*-shRNA-transfected cells intradermally and tumor sizes were measured. Tumor sizes did not significantly differ among these three groups (Fig. 4).

Discussion

The PcG genes encode a family of evolutionarily conserved regulators that were discovered in *Drosophila* as repressors of homoeotic genes, which are involved in establishing body segmentation patterns during development. In mammalian systems, PcG proteins regulate genes involved in development

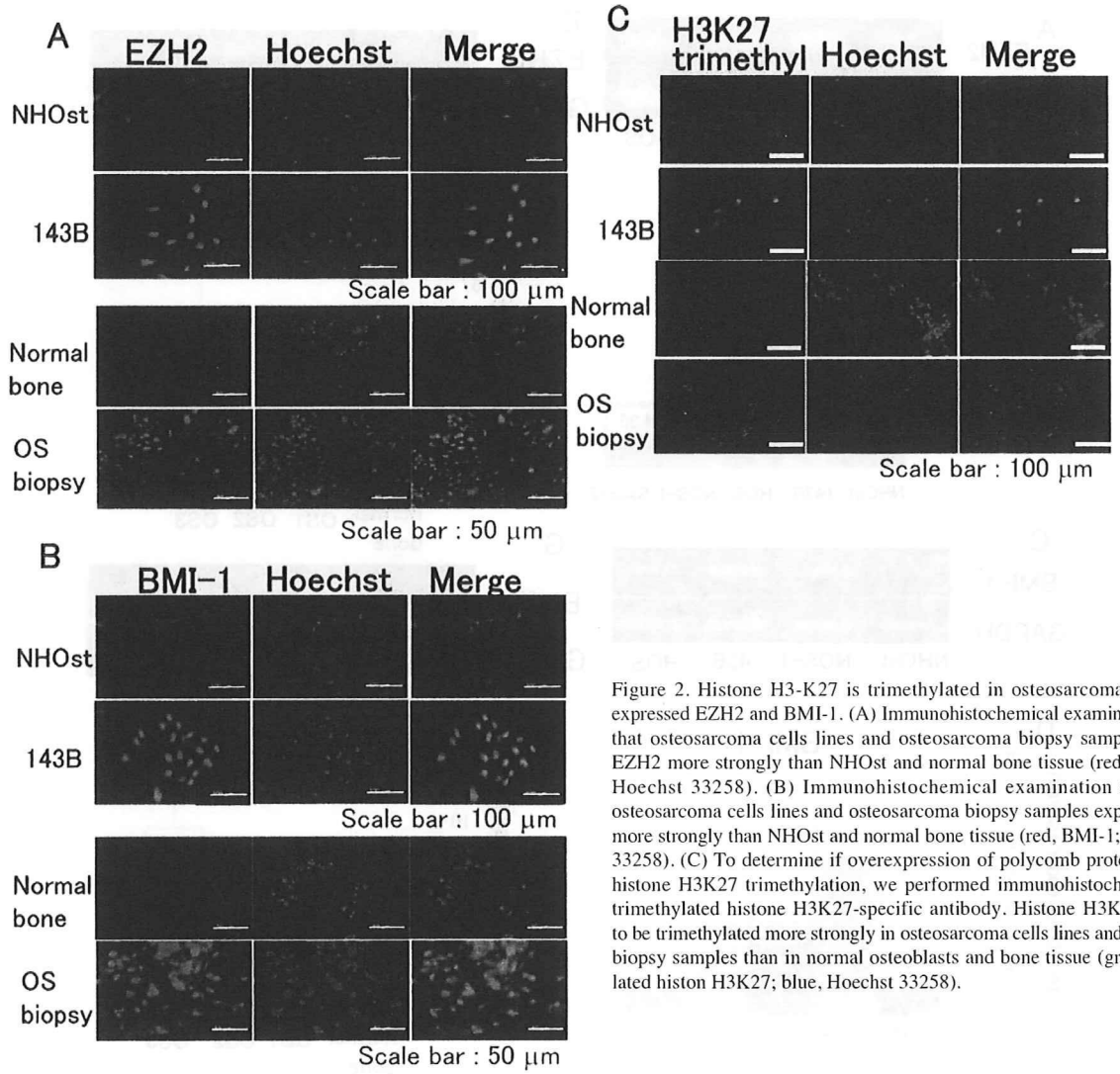

Figure 2. Histone H3-K27 is trimethylated in osteosarcoma which overexpressed EZH2 and BMI-1. (A) Immunohistochemical examination revealed that osteosarcoma cells lines and osteosarcoma biopsy samples expressed EZH2 more strongly than NHOst and normal bone tissue (red, EZH2; blue, Hoechst 33258). (B) Immunohistochemical examination revealed that osteosarcoma cells lines and osteosarcoma biopsy samples expressed BMI-1 more strongly than NHOst and normal bone tissue (red, BMI-1; blue, Hoechst 33258). (C) To determine if overexpression of polycomb proteins promoted histone H3K27 trimethylation, we performed immunohistochemistry using trimethylated histone H3K27-specific antibody. Histone H3K27 was found to be trimethylated more strongly in osteosarcoma cells lines and osteosarcoma biopsy samples than in normal osteoblasts and bone tissue (green, trimethylated histon H3K27; blue, Hoechst 33258).

and differentiation via epigenetic mechanisms. Transcriptional profiling of human tumor samples holds significant promise for the advancement of cancer therapy, both in terms of improving diagnosis as well as predicting patient responses to treatment. Recently, an RNA expression signature associated with 'stem-cell-ness', based partly on PcGs-driven transcriptional changes, was postulated to predict poor therapeutic outcome in patients with various types of cancers (48). Although these claims await further validation, they suggest that levels of PcGs expression might prove valuable as prognostic markers, particularly because *EZH2* and *BMI-1* overexpression appears to be tightly correlated with poor prognosis in various types of cancers (49,50). *BMI-1* was originally identified as an oncogene (8). *BMI-1* up-regulation induces development of B- and T-cell lymphomas (7,41,42). In this study, we found that *EZH2* and *BMI-1* RNAs are up-regulated in osteosarcoma cell lines and patient samples, following the study of overexpression of *EZH2* in the U2OS human osteosarcoma cell line (51). Steele *et al* reported that $CD8^+$ T-cell epitopes derived from EZH2 and BMI-1 elicited T-cell responses as assessed by IFN-γ release confirming the presence of CD8 responses against these proteins in patients with cancer (52). These findings suggest that EZH2 and BMI-1 may be useful targets for cancer immunotherapy of osteosarcoma.

The PRC2 containing EZH2 controls gene repression through recruitment of histone deacetylase. This recruitment leads to local chromatin deacetylation and subsequent trimethylation of Lys_{27} of histone H3 (H3K27). Histone H3K27 trimethylation is a property of stably silenced heterochromatin. The PRC1 complex containing BMI-1 subsequently binds to histone H3K27, suppresses gene expression and contributes to the maintenance of epigenetic memory (53). In this study, we found that histone H3K27 was trimethylated both in osteosarcoma cell lines and patient samples. These findings suggest the possibility that overexpressed EZH2 and BMI-1 are functionally active and promote histone H3K27 trimethylation in osteosarcoma as in stem cells and other types of cancer cells (45,54,55). In addition, trimethylated histone H3K27 suppresses target gene expression via epigenetic regulation (45,55,56). The gene suppression may contribute to the pathogenesis of osteosarcoma. BMI-1 represses the transcription of cell cycle repressors encoded by the ink4a locus (41,57-59). Although PcG proteins are generally

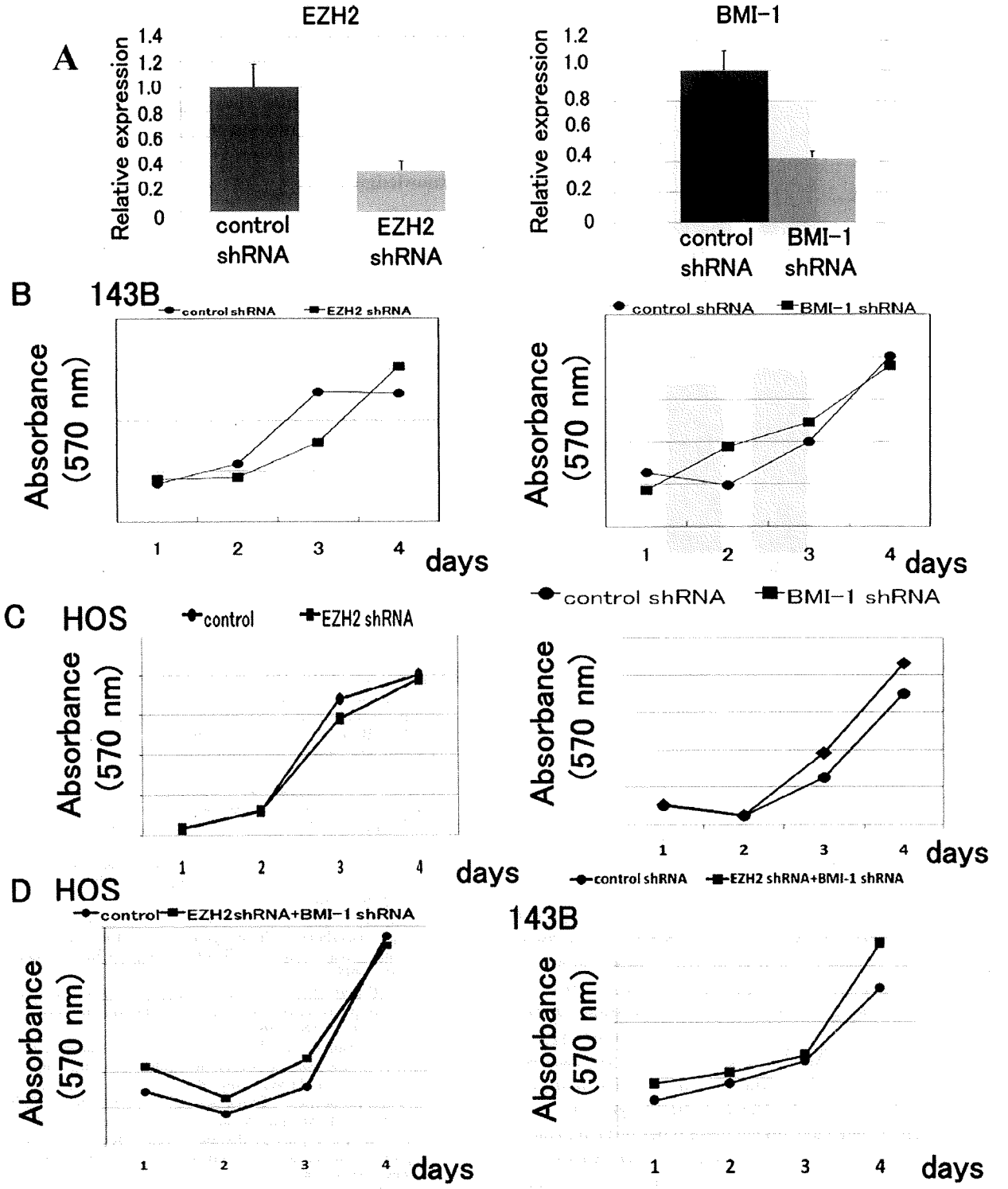

Figure 3. the knock-down of *EZH2* and *BMI-1* does not inhibit osteosarcoma growth *in vitro*. (A) 143B cells were transfected with *EZH2* shRNA and *BMI-1* shRNA. Real-time PCR revealed the knock-down effect by *EZH2* shRNA or *BMI-1* shRNA. (B) MTT assay showed that knock down of *EZH2* and *BMI-1* did not prevent 143B growth *in vitro*. (C) MTT assay showed that knock down of *EZH2* and *BMI-1* did not prevent HOS growth *in vitro*. (D) Double knock-down of *EZH2* plus *BMI-1* did not prevent HOS and 143B growth *in vitro*.

recognized as suppressors of target gene transcription, Shi *et al* reported that EZH2 enhances the transcription of c-myc and cyclin D1 (60). We previously found that transcription of c-myc is activated and expression of the ink4a locus are suppressed in osteosarcoma (61). These findings suggest that these genes may be targets of *EZH2* and *BMI-1* in osteosarcoma.

It has been reported that overexpression of *EZH2* or *BMI-1* promotes malignant transformation (21,36,38,40-47,49). In addition, inhibition of *EZH2* or *BMI-1* inhibits growth of various types of malignancies (38,41-43,45,46,49). These findings suggest that *EZH2* and *BMI-1* play roles in regulating cell proliferation and survival and that *EZH2* or *BMI-1* may be useful as molecular targets in various types of malignancies.

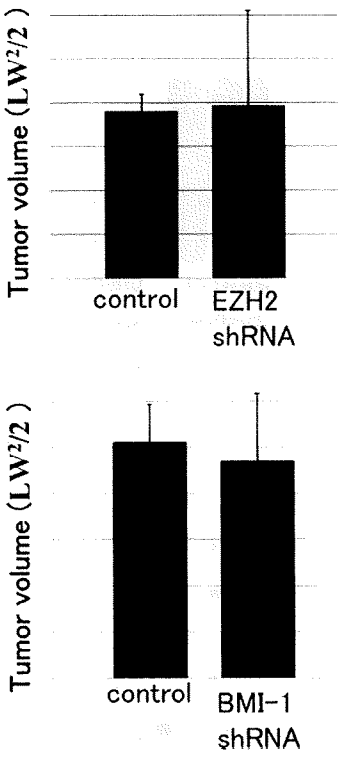

Figure 4. The knock-down of *EZH2* and *BMI-1* does not inhibit osteosarcoma growth *in vivo*. (A) Control shRNA-transfected 143B cells, *EZH2*-shRNA-transfected 143B cells and *BMI-1*-shRNA-transfected cells ($1x10^5$) were inoculated subcutaneously. Established 143B tumors were measured. The tumor volume was evaluated 5 weeks after transplantation (n=3, each group. Error bar, mean standard division).

In fact, pharmacologic interference of EZH2 function induces selective apoptosis of cancer cells but not normal cells (62). In the present study, we examined the effect of *EZH2* and *BMI-1* knock-down in osteosarcoma and found unexpectedly that *EZH2* or *BMI-1* knock-down by shRNA did not prevent osteosarcoma growth *in vitro* or *in vivo*. These findings are contrary to those reported in previous studies. Two groups reported that although PcG protein overexpression appeared to be correlated with poor prognosis for some types of malignancies, low BMI-1 expression was correlated with poor prognosis of endometrial carcinomas and malignant melanocytic lesion (63,64). These studies suggest that osteosarcoma may be included among these types of malignancies. In addition, McGarvey *et al* reported that *EZH2* knock-down results in increased expression of unmethylated and basally expressing genes but not of completely silenced and hypermethylated tumor suppressor genes (65). These findings suggest that important regulator genes for osteosarcoma growth may be hypermethylated. *BMI-1* co-overexpression with other inducers, such as *H-RAS*, *hTERT* and $p16^{INK4a}$ shRNA, resulted in efficient malignant transformation (36,40,41,44). These findings in turn suggest that other factors might be regulated in addition to *BMI-1* to suppress osteosarcoma growth. Taken together, these findings suggest that inhibition of PcG proteins may not be useful for treatment of some other malignancies in addition to osteosarcoma.

In conclusion, we found that *EZH2* and *BMI-1* are up-regulated in osteosarcoma. *EZH2* and *BMI-1* may be useful targets for cancer immunotherapy of osteosarcoma, although knock-down of *EZH2* and *BMI-1* could not prevent osteosarcoma growth. Further investigation of the functions of EZH2 and BMI-1 in osteosarcoma is needed.

Acknowledgements

This study was supported by Grants-in-Aid for Scientific Research (B) 18390419, (C) 19591725, Grant of Japan Orthopaedics and Traumatology Foundation, Inc. No. 0099 and No. 0145 and the Nakatomi Foundation.

References

1. Gibbs CP Jr, Weber K and Scarborough MT: Malignant bone tumors. Instr Course Lect 51: 413-428, 2002.
2. Satijn DP and Otte AP: Polycomb group protein complexes: do different complexes regulate distinct target genes? Biochim Biophys Acta 1447: 1-16, 1999.
3. Otte AP and Kwaks TH: Gene repression by Polycomb group protein complexes: a distinct complex for every occasion? Curr Opin Genet Dev 13: 448-454, 2003.
4. Satijn DP, Gunster MJ, van der Vlag J, *et al*: RING1 is associated with the polycomb group protein complex and acts as a transcriptional repressor. Mol Cell Biol 17: 4105-4113, 1997.
5. Schoorlemmer J, Marcos-Gutierrez C, Were F, *et al*: Ring1A is a transcriptional repressor that interacts with the Polycomb-M33 protein and is expressed at rhombomere boundaries in the mouse hindbrain. EMBO J 16: 5930-5942, 1997.
6. Gunster MJ, Satijn DP, Hamer KM, *et al*: Identification and characterization of interactions between the vertebrate polycomb-group protein BMI1 and human homologs of polyhomeotic. Mol Cell Biol 17: 2326-2335, 1997.
7. Alkema MJ, Bronk M, Verhoeven E, Otte A, van't Veer LJ, Berns A and van Lohuizen M: Identification of Bmi1-interacting proteins as constituents of a multimeric mammalian polycomb complex. Genes Dev 11: 226-240, 1997.
8. van Lohuizen M, Tijms M, Voncken JW, Schumacher A, Magnuson T and Wientjens E: Interaction of mouse polycomb-group (Pc-G) proteins Enx1 and Enx2 with Eed: indication for separate Pc-G complexes. Mol Cell Biol 18: 3572-3579, 1998.
9. Hashimoto N, Brock HW, Nomura M, *et al*: RAE28, BMI1, and M33 are members of heterogeneous multimeric mammalian Polycomb group complexes. Biochem Biophys Res Commun 245: 356-365, 1998.
10. Satijn DP and Otte AP: RING1 interacts with multiple Polycomb-group proteins and displays tumorigenic activity. Mol Cell Biol 19: 57-68, 1999.
11. Bardos JI, Saurin AJ, Tissot C, Duprez E and Freemont PS: HPC3 is a new human polycomb orthologue that interacts and associates with RING1 and Bmi1 and has transcriptional repression properties. J Biol Chem 275: 28785-28792, 2000.
12. Ng J, Hart CM, Morgan K and Simon JA: A *Drosophila* ESC-E(Z) protein complex is distinct from other polycomb group complexes and contains covalently modified ESC. Mol Cell Biol 20: 3069-3078, 2000.
13. Satijn DP, Hamer KM, den Blaauwen J and Otte AP: The polycomb group protein EED interacts with YY1, and both proteins induce neural tissue in Xenopus embryos. Mol Cell Biol 21: 1360-1369, 2001.
14. Tie F, Furuyama T, Prasad-Sinha J, Jane E and Harte PJ: The *Drosophila* Polycomb Group proteins ESC and E(Z) are present in a complex containing the histone-binding protein p55 and the histone deacetylase RPD3. Development 128: 275-286, 2001.
15. Furuyama T, Tie F and Harte PJ: Polycomb group proteins ESC and E(Z) are present in multiple distinct complexes that undergo dynamic changes during development. Genesis 35: 114-124, 2003.
16. Cao R, Wang L, Wang H, *et al*: Role of histone H3 lysine 27 methylation in Polycomb-group silencing. Science 298: 1039-1043, 2002.

17. Czermin B, Melfi R, McCabe D, Seitz V, Imhof A and Pirrotta V: *Drosophila* enhancer of Zeste/ESC complexes have a histone H3 methyltransferase activity that marks chromosomal Polycomb sites. Cell 111: 185-196, 2002.
18. Kuzmichev A, Nishioka K, Erdjument-Bromage H, Tempst P and Reinberg D: Histone methyltransferase activity associated with a human multiprotein complex containing the Enhancer of Zeste protein. Genes Dev 16: 2893-2905, 2002.
19. Muller J, Hart CM, Francis NJ, *et al*: Histone methyltransferase activity of a *Drosophila* Polycomb group repressor complex. Cell 111: 197-208, 2002.
20. Glinsky GV: Genomic models of metastatic cancer: functional analysis of death-from-cancer signature genes reveals aneuploid, anoikis-resistant, metastasis-enabling phenotype with altered cell cycle control and activated Polycomb Group (PcG) protein chromatin silencing pathway. Cell Cycle 5: 1208-1216, 2006.
21. Kleer CG, Cao Q, Varambally S, *et al*: EZH2 is a marker of aggressive breast cancer and promotes neoplastic transformation of breast epithelial cells. Proc Natl Acad Sci USA 100: 11606-11611, 2003.
22. Raaphorst FM, Meijer CJ, Fieret E, *et al*: Poorly differentiated breast carcinoma is associated with increased expression of the human polycomb group EZH2 gene. Neoplasia 5: 481-488, 2003.
23. Breuer RH, Snijders PJ, Smit EF, *et al*: Increased expression of the EZH2 polycomb group gene in BMI-1-positive neoplastic cells during bronchial carcinogenesis. Neoplasia 6: 736-743, 2004.
24. Sudo T, Utsunomiya T, Mimori K, *et al*: Clinicopathological significance of EZH2 mRNA expression in patients with hepatocellular carcinoma. Br J Cancer 92: 1754-1758, 2005.
25. Weikert S, Christoph F, Kollermann J, Muller M, Schrader M, Miller K and Krause H: Expression levels of the EZH2 polycomb transcriptional repressor correlate with aggressiveness and invasive potential of bladder carcinomas. Int J Mol Med 16: 349-353, 2005.
26. Mimori K, Ogawa K, Okamoto M, Sudo T, Inoue H and Mori M: Clinical significance of enhancer of zeste homolog 2 expression in colorectal cancer cases. Eur J Surg Oncol 31: 376-380, 2005.
27. van Kemenade FJ, Raaphorst FM, Blokzijl T, *et al*: Coexpression of BMI-1 and EZH2 polycomb-group proteins is associated with cycling cells and degree of malignancy in B-cell non-Hodgkin lymphoma. Blood 97: 3896-3901, 2001.
28. Visser HP, Gunster MJ, Kluin-Nelemans HC, *et al*: The Polycomb group protein EZH2 is upregulated in proliferating, cultured human mantle cell lymphoma. Br J Haematol 112: 950-958, 2001.
29. Dukers DF, van Galen JC, Giroth C, *et al*: Unique polycomb gene expression pattern in Hodgkin's lymphoma and Hodgkin's lymphoma-derived cell lines. Am J Pathol 164: 873-881, 2004.
30. Raaphorst FM, van Kemenade FJ, Blokzijl T, *et al*: Coexpression of BMI-1 and EZH2 polycomb group genes in Reed-Sternberg cells of Hodgkin's disease. Am J Pathol 157: 709-715, 2000.
31. Bea S, Tort F, Pinyol M, *et al*: BMI-1 gene amplification and overexpression in hematological malignancies occur mainly in mantle cell lymphomas. Cancer Res 61: 2409-2412, 2001.
32. Vonlanthen S, Heighway J, Altermatt HJ, *et al*: The bmi-1 oncoprotein is differentially expressed in non-small cell lung cancer and correlates with INK4A-ARF locus expression. Br J Cancer 84: 1372-1376, 2001.
33. Kim JH, Yoon SY, Kim CN, *et al*: The Bmi-1 oncoprotein is overexpressed in human colorectal cancer and correlates with the reduced p16INK4a/p14ARF proteins. Cancer Lett 203: 217-224, 2004.
34. Mihara K, Chowdhury M, Nakaju N, *et al*: Bmi-1 is useful as a novel molecular marker for predicting progression of myelodysplastic syndrome and patient prognosis. Blood 107: 305-308, 2006.
35. Song LB, Zeng MS, Liao WT, *et al*: Bmi-1 is a novel molecular marker of nasopharyngeal carcinoma progression and immortalizes primary human nasopharyngeal epithelial cells. Cancer Res 66: 6225-6232, 2006.
36. Datta S, Hoenerhoff MJ, Bommi P, *et al*: Bmi-1 cooperates with H-Ras to transform human mammary epithelial cells via dysregulation of multiple growth-regulatory pathways. Cancer Res 67: 10286-10295, 2007.
37. Yang J, Chai L, Liu F, *et al*: Bmi-1 is a target gene for SALL4 in hematopoietic and leukemic cells. Proc Natl Acad Sci USA 104: 10494-10499, 2007.
38. Wiederschain D, Chen L, Johnson B, *et al*: Contribution of polycomb homologues Bmi-1 and Mel-18 to medulloblastoma pathogenesis. Mol Cell Biol 27: 4968-4979, 2007.
39. Hotta T, Motoyama T and Watanabe H: Three human osteosarcoma cell lines exhibiting different phenotypic expressions. Acta Pathol Jpn 42: 595-603, 1992.
40. Haga K, Ohno S, Yugawa T, *et al*: Efficient immortalization of primary human cells by p16INK4a-specific short hairpin RNA or Bmi-1, combined with introduction of hTERT. Cancer Sci 98: 147-154, 2007.
41. Jacobs JJ, Kieboom K, Marino S, DePinho RA and van Lohuizen M: The oncogene and Polycomb-group gene bmi-1 regulates cell proliferation and senescence through the ink4a locus. Nature 397: 164-168, 1999.
42. Jacobs JJ, Scheijen B, Voncken JW, Kieboom K, Berns A and van Lohuizen M: Bmi-1 collaborates with c-Myc in tumorigenesis by inhibiting c-Myc-induced apoptosis via INK4a/ARF. Genes Dev 13: 2678-2690, 1999.
43. Lessard J and Sauvageau G: Bmi-1 determines the proliferative capacity of normal and leukaemic stem cells. Nature 423: 255-260, 2003.
44. Saito M, Handa K, Kiyono T, *et al*: Immortalization of cementoblast progenitor cells with Bmi-1 and TERT. J Bone Miner Res 20: 50-57, 2005.
45. Tonini T, D'Andrilli G, Fucito A, Gaspa L and Bagella L: Importance of Ezh2 polycomb protein in tumorigenesis process interfering with the pathway of growth suppressive key elements. J Cell Physiol 214: 295-300, 2008.
46. Varambally S, Dhanasekaran SM, Zhou M, *et al*: The polycomb group protein EZH2 is involved in progression of prostate cancer. Nature 419: 624-629, 2002.
47. Sellers WR and Loda M: The EZH2 polycomb transcriptional repressor - a marker or mover of metastatic prostate cancer? Cancer Cell 2: 349-350, 2002.
48. Glinsky GV, Berezovska O and Glinskii AB: Microarray analysis identifies a death-from-cancer signature predicting therapy failure in patients with multiple types of cancer. J Clin Invest 115: 1503-1521, 2005.
49. Bracken AP, Pasini D, Capra M, Prosperini E, Colli E and Helin K: EZH2 is downstream of the pRB-E2F pathway, essential for proliferation and amplified in cancer. EMBO J 22: 5323-5335, 2003.
50. Kanno R, Janakiraman H and Kanno M: Epigenetic regulator polycomb group protein complexes control cell fate and cancer. Cancer Sci 99: 1077-1084, 2008.
51. Vire E, Brenner C, Deplus R, *et al*: The Polycomb group protein EZH2 directly controls DNA methylation. Nature 439: 871-874, 2006.
52. Steele JC, Torr EE, Noakes KL, *et al*: The polycomb group proteins, BMI-1 and EZH2, are tumour-associated antigens. Br J Cancer 95: 1202-1211, 2006.
53. Fischle W, Wang Y, Jacobs SA, Kim Y, Allis CD and Khorasanizadeh S: Molecular basis for the discrimination of repressive methyl-lysine marks in histone H3 by Polycomb and HP1 chromodomains. Genes Dev 17: 1870-1881, 2003.
54. Schlesinger Y, Straussman R, Keshet I, *et al*: Polycomb-mediated methylation on Lys27 of histone H3 pre-marks genes for de novo methylation in cancer. Nat Genet 39: 232-236, 2007.
55. Cao R and Zhang Y: The functions of E(Z)/EZH2-mediated methylation of lysine 27 in histone H3. Curr Opin Genet Dev 14: 155-164, 2004.
56. Kondo Y, Shen L, Cheng AS, *et al*: Gene silencing in cancer by histone H3 lysine 27 trimethylation independent of promoter DNA methylation. Nat Genet 40: 741-750, 2008.
57. Silva J, Garcia JM, Pena C, *et al*: Implication of polycomb members Bmi-1, Mel-18, and Hpc-2 in the regulation of p16INK4a, p14ARF, h-TERT, and c-Myc expression in primary breast carcinomas. Clin Cancer Res 12: 6929-6936, 2006.
58. Pardal R, Molofsky AV, He S and Morrison SJ: Stem cell self-renewal and cancer cell proliferation are regulated by common networks that balance the activation of proto-oncogenes and tumor suppressors. Cold Spring Harb Symp Quant Biol 70: 177-185, 2005.
59. Gil J and Peters G: Regulation of the INK4b-ARF-INK4a tumour suppressor locus: all for one or one for all. Nat Rev Mol Cell Biol 7: 667-677, 2006.

60. Shi B, Liang J, Yang X, *et al*: Integration of estrogen and Wnt signaling circuits by the polycomb group protein EZH2 in breast cancer cells. Mol Cell Biol 27: 5105-5119, 2007.
61. Tanaka M, Setoguchi T, Hirotsu M, Gao H, Sasaki H, Matsunoshita Y and Komiya S: Inhibition of Notch pathway prevents osteosarcoma growth by cell cycle regulation. Br J Cancer 100: 1957-1965, 2009.
62. Tan J, Yang X, Zhuang L, *et al*: Pharmacologic disruption of Polycomb-repressive complex 2-mediated gene repression selectively induces apoptosis in cancer cells. Genes Dev 21: 1050-1063, 2007.
63. Engelsen IB, Mannelqvist M, Stefansson IM, *et al*: Low BMI-1 expression is associated with an activated BMI-1-driven signature, vascular invasion, and hormone receptor loss in endometrial carcinoma. Br J Cancer 98: 1662-1669, 2008.
64. Bachmann IM, Puntervoll HE, Otte AP and Akslen LA: Loss of BMI-1 expression is associated with clinical progress of malignant melanoma. Mod Pathol 21: 583-590, 2008.
65. McGarvey KM, Greene E, Fahrner JA, Jenuwein T and Baylin SB: DNA methylation and complete transcriptional silencing of cancer genes persist after depletion of EZH2. Cancer Res 67: 5097-5102, 2007.

MOLECULAR CANCER

RESEARCH Open Access

Smoothened as a new therapeutic target for human osteosarcoma

Masataka Hirotsu†, Takao Setoguchi*†, Hiromi Sasaki†, Yukihiro Matsunoshita, Hui Gao, Hiroko Nagao, Osamu Kunigou, Setsuro Komiya

Abstract

Background: The Hedgehog signaling pathway functions as an organizer in embryonic development. Recent studies have demonstrated constitutive activation of Hedgehog pathway in various types of malignancies. However, it remains unclear how Hedgehog pathway is involved in the pathogenesis of osteosarcoma. To explore the involvement of aberrant Hedgehog pathway in the pathogenesis of osteosarcoma, we investigated the expression and activation of Hedgehog pathway in osteosarcoma and examined the effect of SMOOTHENED (SMO) inhibition.

Results: To evaluate the expression of genes of Hedgehog pathway, we performed real-time PCR and immunohistochemistry using osteosarcoma cell lines and osteosarcoma biopsy specimens. To evaluate the effect of SMO inhibition, we did cell viability, colony formation, cell cycle *in vitro* and xenograft model *in vivo*. Real-time PCR revealed that osteosarcoma cell lines over-expressed *Sonic hedgehog*, *Indian hedgehog*, *PTCH1*, *SMO*, and *GLI*. Real-time PCR revealed over-expression of *SMO*, *PTCH1*, and *GLI2* in osteosarcoma biopsy specimens. These findings showed that Hedgehog pathway is activated in osteosarcomas. Inhibition of SMO by cyclopamine, a specific inhibitor of SMO, slowed the growth of osteosarcoma in vitro. Cell cycle analysis revealed that cyclopamine promoted G1 arrest. Cyclopamine reduced the expression of accelerators of the cell cycle including cyclin D1, cyclin E1, SKP2, and pRb. On the other hand, $p21^{cip1}$ wprotein was up-regulated by cyclopamine treatment. In addition, knockdown of *SMO* by *SMO* shRNA prevents osteosarcoma growth in vitro and in vivo.

Conclusions: These findings suggest that inactivation of SMO may be a useful approach to the treatment of patients with osteosarcoma.

Background

Osteosarcoma is the most common primary bone malignant tumor occurring mainly in children [1]. After initial diagnosis is made by biopsy, treatment consists of preoperative chemotherapy, followed by definitive surgery and postoperative chemotherapy. Survival has improved over the past several decades. Indeed, patients with non-metastatic disease have a 70% chance of long-term survival. Unfortunately, patients with metastatic disease at diagnosis and those who have recurrent disease have a poor prognosis, with only 20% surviving at 5 years, indicating that new therapeutic options for them need to be actively explored. In cancer cells, dysregulation of cell division and apoptotic processes contribute to both drug resistance and metastatic potential [2,3]. It has been reported that inactivation of the cell cycle regulatory pathway centered around the Rb gene is a critical step in the pathogenesis of osteosarcoma [4]. Although such dysregulation may constitute a potent source of new therapeutic targets, the molecular mechanisms of regulation of osteosarcoma cell proliferation are largely unknown.

Hedgehog (Hh) pathway has been implicated in different aspects of animal development, acting through several components, including the transmembrane proteins PATCHED (PTCH1) and SMOOTHENED (SMO), to activate the GLI zinc-finger transcription factors [5,6]. Hh pathway is critical for many processes during embryonic and postnatal development, including proliferation, differentiation, specification of cell fate,

* Correspondence: setoro@m2.kufm.kagoshima-u.ac.jp
† Contributed equally
Department of Orthopaedic Surgery, Graduate School of Medical and Dental Sciences, Kagoshima University, Kagoshima, 890-8520, Japan

left-right asymmetry, and morphogenesis [7]. Sporadic and familial mutations in the Hh pathway genes, PTCH1, suppressor-of-fused, and SMO, leading to elevated expression of downstream target genes including GLI, have been reported in basal cell carcinoma and the pediatric brain tumor medulloblastoma [8,9]. In addition, the growth of many cancers has been suggested to depend on continuous Hh pathway even in the absence of activating mutations in the pathway (reviewed in ref. [10]).

To explore the involvement of Hh pathway in the pathogenesis of osteosarcoma, we investigated the expression and activation of the Hh pathway genes in osteosarcoma and examined the effect of inhibition of SMO by cyclopamine, a specific inhibitor of SMO [11] or *SMO* shRNA.

Results

Over-expression of Hh-GLI pathway molecules in osteosarcoma

To examine the role of Hhï¿½GLI pathway in osteosarcoma, we tested for the expression of Hh in osteosarcoma cell lines. Real-time PCR revealed that 4 of 5 human osteosarcoma cell lines increased *Sonic Hedgehog* (*SHH*) 2.1- to 18.8-fold (Fig. 1). In addition, 5 of 5 osteosarcoma cell lines increased *Desert Hedgehog* 1.3- to 24.4-fold (Fig. 1). To further examine Hh pathway molecules expression, we performed real-time PCR for Hh receptors and Hh target genes. *PTCH1* was up-regulated 2.7-to 65.8-fold in 5 of 5 human osteosarcoma cell lines. *SMO* was up-regulated 2.1-to 5.8-fold in 4 of 5 human osteosarcoma cell lines. *SMO* was up-regulated 2.1-to 5.8-fold in 4 of 5 human osteosarcoma cell lines. *GLI1* was up-regulated 2.5-to 8.9-fold in 5 of 5 human osteosarcoma cell lines. *GLI2* was up-regulated 1.2-to 9.9-fold in 5 of 5 human osteosarcoma cell lines. To extend these findings, we performed immunocytochemistry for SMO and GLI2, and found that only osteosarcoma cells expressed detectable levels of SMO and GLI2. GLI2 was located in the nuclei of osteosarcoma cells (see additional file 1). We next examined *SMO* expression in osteosarcoma patient' biopsy specimens. Real-time PCR revealed that 9 of 9 human biopsy specimens of osteosarcoma increased *SMO* 1.44- to 55.5-fold (Fig. 2). In addition, real-time PCR revealed that expression of *PTCH1* was increased in 8 of 9 patients' biopsy samples 2.44- to 29.4-fold (Fig. 2). *GLI2* was up-regulated 2.5-to 58.4-fold in 9 of 9 human biopsy specimens of osteosarcoma (Fig. 2). Of most importance was the finding that markers of active Hhï¿½GLI signaling, *GLI2* and *PTCH1* were consistently up-regulated in the examined osteosarcoma cells, demonstrating the aberrant Hh-GLI pathway activation [12-14]. Our findings suggest that Hh-GLI signaling is active in osteosarcomas.

Inhibition of SMO prevents osteosarcoma growth in vitro

To determine whether activation of Hh-GLI signaling is required for osteosarcoma cell growth, we used cyclopamine, a pharmacological agent known to effectively block Hh-GLI signaling by inhibiting SMO activation [11]. We performed real-time PCR to determine whether cyclopamine effectively inhibited the expression of the GLI target gene *PTCH1* and *GLI2* [14]. Cyclopamine at 20 μM reduced mRNA levels of *PTCH1* and *GLI2* in osteosarcoma cells by more than 60%, consistent with the expected down-regulation of Hh-GLI signaling (Fig. 3A). As cyclopamine was used to prevent cancer cells growth at 10 to 20 μM [15-17] we decided 20 μM was appropriate concentration for osteosarcoma. MTT assay showed that cyclopamine slowed the growth of HOS and 143B in dose-dependent fashion (Fig. 3B). On the other hand, MTT assay showed that proliferation of osteosarcoma cells was enhanced by SHH. We next used a clonogenic assay to determine whether cells capable of forming anchorage-independent colonies were depleted by cyclopamine. This assay revealed cyclopamine reduced colony formation in soft agar (Fig. 3C). These findings suggest that inhibition of SMO inhibited osteosarcoma growth in vitro.

Hh signaling regulates cell cycle of osteosarcoma

We examined cell cycle characteristics by flow cytometry. Of 143B cells cultured without cyclopamine, 39.8% of cells were in G1 phase, while 56.6% of cells were in G1 phase following treatment with cyclopamine. In the case of HOS cells were cultured without cyclopamine, 55.4% cells were in G1 phase. On the other hand, when cultured with cyclopamine, 72.3% of cells were in G1 phase (Fig. 4A). These findings suggested that cyclopamine promoted G1 arrest. We then examined the transcription of cell cycle-related genes. Real-time PCR revealed that cyclopamine prevented the transcription of accelerators of the cell cycle including *cyclin D1*, *cyclin E1*, *SKP2*, and *NMYC* (Fig. 4B). In mammalian cells, cyclin D, cyclin E, and $p21^{cip1}$ are short-lived proteins that are controlled by ubiquitin-dependent proteolysis. We performed western blot analysis to determine protein levels, and found that cyclopamine reduced the levels of expression of cyclin D1 and cyclin E1 proteins. Cyclopamine also reduced the levels of expression of cyclin D1, cyclin E1, pRb, and SKP2 proteins (Fig. 4C). We next examined the expression of $p21^{cip1}$, and found that $p21^{cip1}$ protein was up-regulated by cyclopamine treatment (Fig. 4C). These findings suggested that cyclopamine promoted G1 arrest by inhibition of G1-S phase progression. These findings suggest that inhibition of SMO inhibited osteosarcoma growth via cell cycle regulation.

Knock down of SMO prevents osteosarcoma growth in vivo

To confirm the effect of SMO suppression, we examined the effect of *SMO* shRNA. 143B was transfected with